A pile-soil interaction model for ground-borne vibration problems based on the singular boundary method

Kenny F. Conto[a,*], Robert Arcos[a,b], Arnau Clot[a,b], Evangelos Ntotsios[c], Hassan Liravi[a], Aires Colaço[d], David J. Thompson[c]

[a]*Acoustical and Mechanical Engineering Laboratory (LEAM), Universitat Politècnica de Catalunya (UPC), c/Colom 11, Terrassa (Barcelona), Spain.*
[b]*Serra Húnter Fellow, Universitat Politècnica de Catalunya (UPC), Spain.*
[c]*Institute of Sound and Vibration Research (ISVR), University of Southampton, Southampton SO17 1BJ, United Kingdom*
[d]*CONSTRUCT-FEUP, University of Porto, Rua Dr. Roberto Frias s/n, 4200-465, Porto, Portugal.*

Abstract

An efficient three-dimensional approach for solving pile-soil interaction problems is proposed. In the approach, the soil is modelled as an elastic half-space, and its response in the presence of the pile's corresponding cavity is computed by employing the singular boundary method. The pile is modelled analytically using the classic rod and Euler-Bernoulli beam theories. For the coupling with the soil, the pile is divided in a set of rigid segments that interact along their circumference with the soil. The methodology allows the rotational motions and reaction torques at these segments to be accounted for and their contribution in the accuracy of the scheme is assessed. A criterion to define the minimum number of collocation points that offers an acceptable trade-off between accuracy and numerical performance is also proposed. The method is validated against well-established methodologies and using the reciprocity principle that relates the wave radiation from the pile to the ground field with the incident wave problem due to a load on the ground surface. Results are shown for different soil stiffnesses and different pile length to diameter ratios. The employment of the singular boundary method is shown to provide strong computational advantages to detailed modelling approaches such as the three-dimensional finite element-boundary element method, as well as overcoming the fundamental limitations of plane-strain and axisymmetric methods.

Keywords: Pile-soil interaction, Single piled-foundation, Singular boundary method (SBM), Soil-structure interaction

1. Introduction

In the last decades, public transport networks in big metropolises have grown rapidly. As a consequence, the proximity of urban transport infrastructures to residential buildings, libraries, hospitals and other civil structures is

*Corresponding author
Email address: kenny.fernando.conto@upc.edu (Kenny F. Conto)

rapidly increasing. Ground-borne vibration induced by, for instance, road and railway traffic or construction activities reach these structures through their foundation, contributing to the noise and vibration pollution of their interior environment. Although the vibration caused by these activities rarely leads to structural damage, it can be a significant cause of annoyance for the building inhabitants or can cause malfunctioning of sensitive devices.

The structural component responsible for the transmission of ground vibration to civil structures is its foundation system. Piled foundation systems are the preferred option among the most common foundation solutions, especially for tall structures or poorly consolidated soils. Over the years, different approaches have been proposed for estimating the dynamic behaviour of the piled foundation system. These approaches are generally based on three modelling strategies: the dynamic Winkler foundation approach, the elastic continuum theory and mesh-based numerical modelling methods. The reader can find a fully comprehensive review of the existing modelling strategies for pile-soil dynamic interaction in [1]. However, to include some recently proposed methodologies and, more importantly, to make prominent what new contribution the present work offers relative to the existing methods, the main capabilities and assumptions of each modelling approach are briefly outlined in the following paragraphs.

Novak's approach [2] is known as the first method that considers the dynamic soil response in pile foundation modelling. In this approach, the pile is modelled as an elastic rod and an Euler-Bernoulli beam, and the soil around the pile is considered as an infinite number of infinitesimally thin horizontal layers perfectly bonded to the pile. The soil layers are dynamically uncoupled from each other, and each layer is modelled by a spring stiffness and damping factor known as the Winkler foundation model. This pile-soil coupling method was based on previous studies on a circular surface and embedded footings [3–6]. Novak's approach was validated against experimental results [7] and is widely used in the field of earthquake engineering; however, although it can predict the in-plane vertical response of a single pile accurately, it presents significant limitations when either the response to a horizontal force applied to the pile, dynamic interaction between piles or the ground field response are required.

To overcome the limitations of the Winkler foundation approach, elastic continuum theory has been considered where the soil is modelled as an elastic half-space, while the pile, similarly with several Winkler-type approaches, is modelled as an axial rod for vertical vibrations and as an Euler-Bernoulli beam for lateral vibrations. One of the most well-known three-dimensional models for single-pile and pile-group problems was developed by Kaynia and Kausel [8], who obtained the dynamic behaviour of pile-soil systems by using dynamic substructuring. To represent the soil reaction, half-space Green's functions using integral transformation techniques associated with two types of translational loading patterns were employed: piecewise cylindrical barrel loads, associated with the soil reaction at the surface of the pile, and circular disk loads, related to the tractions at the pile tip. In a similar approach [9], translational and rotational ring line loads at a discrete number of soil-pile interaction layers were proposed to include the

traction moments of the coupled system. Other examples of the elastic-continuum-type formulation include Nogami and Novak [10–12], Pak and Jennings [13], Wolf [14], Rajapakse and Shah [15, 16] , Anoyatis et al. [17, 18] and Di laora et al. [19, 20]. While these analytical elastic-continuum formulations are more accurate than Winkler-type models to model pile foundation under harmonic loads or kinematic interactions, soil inhomogeneity can only be included in the form of layers or varying elastic moduli. Moreover, the soil cavity is not explicitly modelled, but rather the pile is treated as reinforcement, with density and elastic modulus equal to the difference between the desired pile and soil values. Kuo and Hunt in [21] have included the soil cavity and proposed a single pile-soil modelling approach which uses the mirror-image method to account for the boundary conditions at the pile head. Nonetheless, that formulation was based on the Pipe-in-Pipe model (PiP) [22, 23] that for the calculation of the soil-pile interaction tractions considers the soil medium as a full-space with a cavity, downplaying the effect of the soil surface and soil inhomogeneity. Despite their limitations, the analytical elastic-continuum methods are quite popular, offering improved computational efficiency over the numerical methods described in the following. Modelling strategies based on numerical methods are suitable when the system has a significant degree of complexity, such as intricate geometries, depth-dependency of the soil mechanical properties [24, 25], non-linear soil behaviour [26–28] or discontinuity conditions at the pile-soil interface [29]. One of the first works on modelling piled foundations employing a numerical method is attributed to Kuhlemeyer [30, 31], who took advantage of the finite element method (FEM) versatility to determine the dynamic response of the system under lateral and vertical loads. Syngros [32] presented a single pile foundation model based on an axisymmetric FE approach to deal with vertical load applied at the pile head. The model used simplified expressions to represent the soil inhomogeneity in vertical and radial directions induced by, respectively, vertical overburden and pile driving. Other examples of single pile systems using the axisymmetric FE approach to model impact pile driving include [33, 34]. Because of the finite nature of the domains that FEM can handle, frequency-dependent [2], or frequency-independent [35] absorbing boundaries were proposed to be included in FE models of soil-structure interaction problems in order to represent the semi-infinite nature of the soil medium by avoiding wave reflections. In contrast, due to its boundary-type discretisation nature, the boundary element method (BEM) can naturally deal with infinite or semi-infinite domains. A review of different BEM-based approaches for two-dimensional (2D) and three-dimensional (3D) elastodynamic problems in time and frequency domains can be found in [36, 37].

A model for piled-foundations entirely based on the BEM was proposed by Kattis et al. in [38], while Padrón et al. [39] proposed a finite element-boundary element (FE-BE) approach in which the pile is modelled by employing the FEM and the surrounding soil using BE. As an alternative for the case of dynamic pile-soil interaction, Talbot and Hunt [40] developed an efficient approach for solving a single pile or an infinite row of piles based on periodic structure theory. In that work, the pile is modelled using the solutions for an elastic bar and Euler beam theory for

vertical and lateral motions, respectively, and is coupled with a BE model of the soil that uses constant rectangular elements for meshing the ground surface and the pile cavity. In [41], Coulier varied the method in [40] by considering a Timoshenko beam model of the pile, showing that the effect is relatively small, and considered multiple piles to study the dynamic response of the piles due to incident wave fields induced by underground railway traffic. Extending the original single pile model by Talbot and Hunt in [40], Edirisinghe and Talbot [42] proposed a methodology for computing the dynamic response of pile groups at higher frequencies. In this methodology, the piles and the soil are considered to be two independent 'weakly-coupled' subsystems where the soil is not accounting for the corresponding cavities associated with the piles. The response of the coupled system is computed by an iterative wave-scattering approach, and the results agreed well with the 'strongly-coupled' model and the model in [8].

Even though models based on those numerical approaches are highly accurate, they present a key disadvantage; they involve considerable computational effort, especially at high frequencies. To mitigate this problem, meshless methods have emerged as an alternative due to their simplicity and their potential to be more computationally efficient than mesh-based approaches. In this context, the singular boundary method (SBM), originally proposed by Chen in [43], has gained popularity these recent years due to its robustness with respect to other meshless approaches. The SBM can be seen as a modified version of the method of fundamental solutions (MFS). In brief, the MFS uses a set of virtual forces, which are computed by ensuring that they satisfy a previously known boundary condition. These boundary conditions are evaluated on a set of points called collocation points. Typically, the MFS considers the placement of the virtual forces outside the domain, whereas the SBM proposes to locate the sources at the physical boundary, superimposed on the collocation points. Like the MFS, the SBM employs the fundamental solutions (or Green's functions) of the governing equation of the problem of interest (e.g. a homogeneous full space or a layered half-space) as the interpolation basis functions. However, singularities of the fundamental solution arise when the collocation points are geometrically coincident with the virtual sources. In those situations, the response is evaluated by the so-called origin intensity factors (OIFs), which overcome the singularity of the fundamental solution for both Neumann and Dirichlet boundary problems.

Although the SBM has been extensively employed for solving problems in acoustics, few investigations are available on the application of the SBM to elastic wave propagation problems. Gu et al. [44] employed the SBM for plane strain elastostatics and later to deal with orthotropic elastostatic problems [45]. This last work also presented a theoretical background for the SBM formulation, stating that the SBM can be seen as a discrete version of the indirect boundary integral equations based on the single-layer potential formulation. In [46] Sun et al. applied the SBM to 2D dynamic poroelastic problems. Recently, Liravi et al. [47] have proposed an approach formulated in the two-and-a-half-dimensional (2.5D) domain for modelling 3D longitudinally invariant soil-structure interaction problems which

employ FE to model the structure while the soil domain is modelled using the SBM. Results presented show that the SBM offers higher computational efficiency than the boundary element method (BEM) and more robustness than the MFS.

Motivated by the aforementioned advantages of the SBM, this paper presents a new approach for computing the dynamic response of a single pile embedded in the soil. Although the formulation presented in this article is developed for a single-pile foundation, it can be easily adapted to deal with pile-group foundation problems by considering multiple piles and cavities in the soil. Herein, the pile is modelled using axial rod theory for vertical and torsional reactions and using Euler-Bernoulli beam theory for accounting for flexural motions, whilst a novel methodology based on the SBM is adopted to model the soil as a half-space medium. A convergence criterion is also proposed to define the minimum number of collocation points that offers an acceptable trade-off between accuracy and numerical performance. The accuracy and computational efficiency of the proposed modelling approach with respect to other existing methodologies are highlighted by comparing the resulting driving-point and transfer receptances of the pile-soil system with results from three state-of-the-art models. These are the dynamic Winkler foundation approach by Novak in [2]; the axisymmetric FE-based approach in [34]; and a 3D FE-BE approach developed on the basis of [48]. In Section 2, the main assumptions and the formulation required for solving each subsystem and their coupling procedure are described. The robustness of the formulation, the convergence analysis, the validation study and the comparison of the computational efficiency with other methods are discussed in Section 3, whilst the conclusions are summarised in Section 4.

2. Single-pile foundation modelling

The system under investigation consists of a single pile embedded in a homogeneous half-space, as shown schematically in Fig. 1, with the origin of the Cartesian coordinate system placed on the ground surface and coincident with the pile axis. In the formulation, lowercase letters denote variables in the time domain, and uppercase letters relate to scalar variables in the frequency domain. Bold lowercase letters and bold uppercase letters denote vectors or matrices in the time domain and frequency domain, respectively. A modelling strategy is presented that aims to compute the dynamic response of the system, at the pile head and at the ground surface, due to loads applied at the pile head and/or at the ground surface. The pile is assumed to be purely elastic and is modelled as a rod to account for axial and torsional motions, whilst the Euler-Bernoulli beam theory is considered for the flexural response of the pile. The soil is considered as an elastic homogeneous half-space; however, the proposed methodology can be applied to layered soils as well. Non-linear effects associated with pile-soil contact interactions, high strain levels or soil liquefaction are not accounted for. The coupled pile-soil model is formulated in the frequency domain and constructed

employing the dynamic substructuring technique; the response of each subsystem is separately derived and they are coupled considering force equilibrium and displacement compatibility conditions. The mathematical formulation of the proposed model is presented in the following subsections.

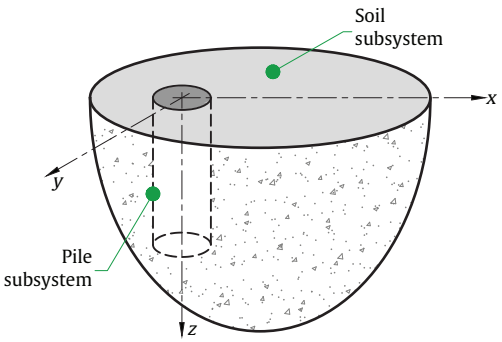

Figure 1: Schematic drawing of the pile-soil system.

2.1. Model of the pile subsystem

As mentioned above, the pile subsystem is modelled analytically using axial rod and Euler-Bernoulli beam theories. Thus, the model accounts for the 3D deformation of the pile, represented by displacements (u_{px}, u_{py}, u_{pz}) and rotations $(\phi_{px}, \phi_{py}, \phi_{pz})$ along the three Cartesian coordinates (x, y, z), respectively. Free-free boundary conditions are adopted for both rod and beam models. In this section, the expressions that determine the response of the pile model when subjected to loads applied to an arbitrary position along the pile axis z are outlined.

First, consider the differential equations of motion of a rod for axial and torsional deformations before applying any external excitation, which are given by the expressions:

$$\rho_p \frac{\partial^2 u_{pz}(z,t)}{\partial t^2} - E_p \frac{\partial^2 u_{pz}(z,t)}{\partial z^2} = 0, \tag{1a}$$

$$\frac{\partial^2 \phi_{pz}(z,t)}{\partial t^2} - C_s^2 \frac{\partial^2 \phi_{pz}(z,t)}{\partial z^2} = 0, \tag{1b}$$

where E_p is the elastic modulus of the pile. The shear wave speed of the pile is given by $C_s = \sqrt{G_p/\rho_p}$, being G_p the shear modulus and ρ_p its density. For the bending motion of the pile, the differential equation of an Euler-Bernoulli beam

$$\rho_p A_p \frac{\partial^2 u_{px}(z,t)}{\partial t^2} + E_p I_p \frac{\partial^4 u_{px}(z,t)}{\partial z^4} = 0, \tag{2}$$

is employed, where A_p is the cross-sectional area of a pile, and I_p is the second moment of area of the pile's cross-section. The same expression is also valid for $u_{py}(z,t)$ that describes the bending in the y direction.

The pile is excited at an arbitrary position z_1 along the pile axis, as illustrated in Fig. 2, by an arbitrary set of harmonic forces and moments of the form $f_i(z,t) = F_i(z)\exp(\mathrm{i}\omega t)$ and $m_i(z,t) = M_i(z)\exp(\mathrm{i}\omega t)$, respectively, with $i = x, y, z$, ω is the angular frequency and $\mathrm{i} = \sqrt{-1}$ represents the unit imaginary number. The resulting displacements and rotations of the pile take the form $u_{\mathrm{p}i}(z,t) = U_{\mathrm{p}i}(z)\exp(\mathrm{i}\omega t)$ and $\phi_{\mathrm{p}i}(z,t) = \theta_{\mathrm{p}i}(z)\exp(\mathrm{i}\omega t)$, respectively, where $\theta_{\mathrm{p}i}$ is used to represent the rotational motion $\phi_{\mathrm{p}i}$ in the frequency domain. As a result, the axial response of the free-free pile along its neutral axis due to a unit point load can be expressed in the frequency domain as

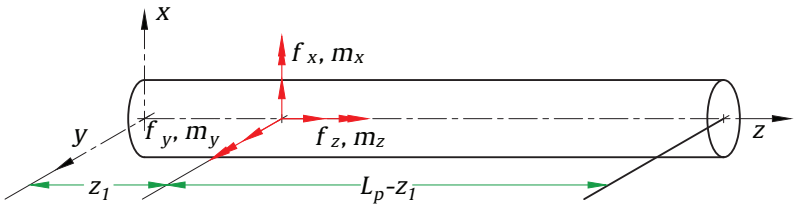

Figure 2: Pile subsystem (illustrated horizontally for convenience) subjected to arbitrary loads at an arbitrary position along the pile axis.

$$U_{\mathrm{p}z}(z) = A_1\cos(\alpha z) + A_2\sin(\alpha z), \qquad 0 \leqslant z \leqslant z_1, \tag{3a}$$

$$U_{\mathrm{p}z}(z) = A_3\cos(\alpha z) + A_4\sin(\alpha z), \qquad z_1 \leqslant z \leqslant L_{\mathrm{p}}, \tag{3b}$$

where L_{p} is the pile length and $\alpha^2 = (\rho_{\mathrm{p}}\omega^2)/E_{\mathrm{p}}$.

Similarly, the expressions for the torsional response are given by

$$\theta_{\mathrm{p}z}(z) = B_1\cos(\gamma z) + B_2\sin(\gamma z), \qquad 0 \leqslant z \leqslant z_1, \tag{4a}$$

$$\theta_{\mathrm{p}z}(z) = B_3\cos(\gamma z) + B_4\sin(\gamma z), \qquad z_1 \leqslant z \leqslant L_{\mathrm{p}}, \tag{4b}$$

where $\gamma^2 = (\rho_{\mathrm{p}}\omega^2)/G_{\mathrm{p}}$. The expressions for the coefficients A_j in Eqs. (3) and B_j in Eqs. (4) can be found in Appendix A.

Finally, the lateral displacements induced by lateral loads or bending moments can be determined using the following expressions:

$$U_{\mathrm{p}x}(z) = C_1\cos(\beta z) + C_2\sin(\beta z) + C_3\cosh(\beta z) + C_4\sinh(\beta z), \qquad 0 \leqslant z \leqslant z_1, \tag{5a}$$

$$U_{\mathrm{p}x}(z) = C_5\cos(\beta z) + C_6\sin(\beta z) + C_7\cosh(\beta z) + C_8\sinh(\beta z), \qquad z_1 \leqslant z \leqslant L_{\mathrm{p}}, \tag{5b}$$

where $\beta^4 = (\rho_p A_p \omega^2)/(E_p I_p)$. The coefficients C_j are again given in detail in Appendix A, whilst the cross-sectional rotation induced by lateral loads or bending moments can be obtained applying $\theta_{py} = \partial U_{px}/\partial z$ in Eq. (5). These expressions are associated with the bending in the y direction: analogous expressions can be used for the bending of the pile in the x direction.

2.2. *Model of the soil subsystem*

The soil subsystem is modelled as an elastic half-space that includes the cavity corresponding to the pile using the SBM [45, 47, 49]. In order to describe the SBM-based model of the soil presented in this work, consider the general case of a 3D cavity in an elastic medium $\Omega \in \mathbb{R}^3$, as shown in Fig. 3(a), where $\partial\Omega$ represents the boundary. In that figure, $\mathbf{x}$ and $\mathbf{y}$ denote points located at $\partial\Omega$ and Ω, respectively. As a radial basis function method, the SBM assumes that the dynamic unknown states of the medium (the displacement and traction fields for the case of the soil) can be approximated by a linear combination of the fundamental solution or Green's function of the medium evaluated at a set of virtual sources placed over the physical boundary $\partial\Omega$. Red circles in Fig. 3(b) and Fig. 3(c) represent this set of virtual forces. This leads to a system of equations that can be expressed as

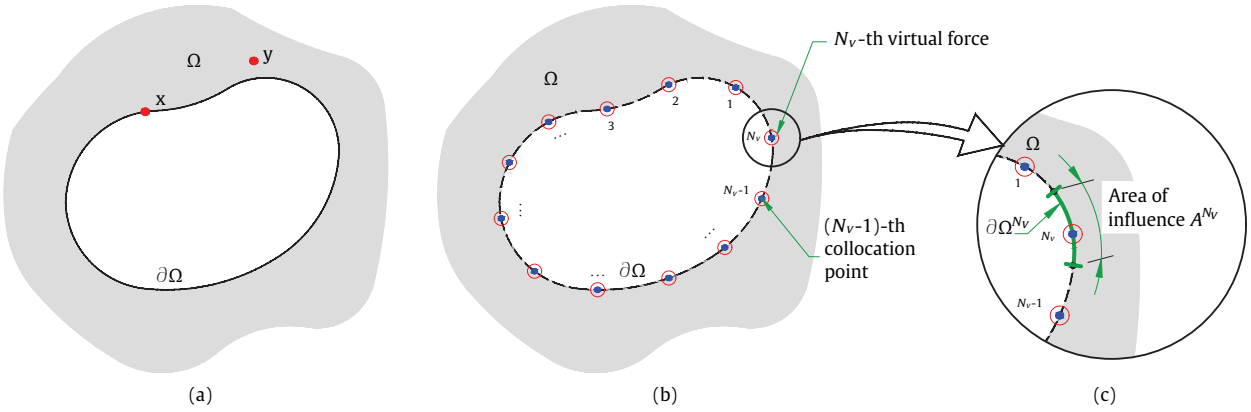

Figure 3: Schematic of the generic problem (a); distribution of the collocation points (marked by blue dots) and the virtual sources (marked by red circles) over the boundary (b); and generic description of the area of influence associated with a particular virtual source (c).

$$\mathbf{U}(\mathbf{y}) = \sum_{v=1}^{N_v} \mathbf{H}(\mathbf{y}, \mathbf{x}^v, \omega)\mathbf{S}^v, \tag{6a}$$

$$\mathbf{T}(\mathbf{y}) = \sum_{v=1}^{N_v} \mathbf{H}^T(\mathbf{y}, \mathbf{x}^v, \omega)\mathbf{S}^v, \tag{6b}$$

where the vectors $\mathbf{U}(\mathbf{y})$, $\mathbf{T}(\mathbf{y})$ contain the three components of the displacements and tractions of the medium, respectively, at the point $\mathbf{y}$. These are induced by a set of virtual sources in which the v-th virtual force of the set is defined by the three-component complex vectors $\mathbf{S}^v$ for amplitude and $\mathbf{x}^v$ for position. The displacement and traction elastodynamic fundamental solutions in the frequency domain evaluated at the point $\mathbf{y}$ caused by a point load placed at $\mathbf{x}^v$ are represented by the matrices $\mathbf{H}(\mathbf{y}, \mathbf{x}^v, \omega)$ and $\mathbf{H}^\tau(\mathbf{y}, \mathbf{x}^v, \omega)$, respectively. Eq. (6) can be seen as a discrete version of the indirect boundary integral equation in the form of a single-layer potential, as discussed in detail by Gu et al. [45]. Thus, the set of virtual sources can be interpreted as a discretization of the flux discontinuity, which is used as auxiliary sources in the indirect boundary integral equations in the form of a single-layer potential [48]. It is worth mentioning that the fundamental solution notation in this paper is based on a function with three input variables: the first representing the receiver location, the second the source location and the third the angular frequency at which the fundamental solution is evaluated. In the case of the traction fundamental solution, the vector normal to the plane at which the traction is evaluated is a variable not explicitly stated in the notation of the fundamental solutions but also required in its calculation.

It is important to note that, as for the BEM, the SBM naturally allows for using Green's functions of more complex problems than the case of a full-space, for instance, homogeneous or layered half-spaces (both employed in [47]). In this work, the soil is assumed to be a homogeneous elastic half-space, and the corresponding Green's functions to this problem are computed on the basis of the direct stiffness matrix method proposed by Kausel [50], although the adoption of layered models of the soil can be carried out simply replacing those Green's functions with the corresponding ones of the adopted layered half-space configuration.

To determine the virtual sources due to the prescribed boundary conditions, the collocation method is commonly used in boundary domain methods, which proposes to discretize those boundary conditions at a set of collocation points distributed along the physical boundary. For the particular SBM approach presented in this work, a set of collocation points, defined by the positions $\mathbf{x}^c$, is established for $c = 1, 2, ..., N_\mathrm{c}$. This set of collocation points is assumed to be geometrically coincident with the set of virtual sources, having $N_\mathrm{c} = N_\mathrm{v}$. Both sets of collocation and source points are shown in Fig. 3(b). A linear system of equations results by the evaluation of Eq. (6) at all the collocation points of the set. Due to geometrical coincidence between collocation and source sets, singularities arise from the fundamental solutions in Eq. (6) when $c = v$. To overcome those singularities, the SBM proposes to employ the origin intensity factors (OIFs) [47]. Equations of the resulting linear systems for Dirichlet and Neumann boundary conditions, respectively, are

$$\mathbf{U}(\mathbf{x}^c) = \sum_{v=1, v\neq c}^{N_\mathrm{v}} \mathbf{H}(\mathbf{x}^c, \mathbf{x}^v, \omega)\mathbf{S}^v + \mathbf{H}_{\mathrm{cc}}\mathbf{S}^c, \quad \text{for } c = 1, 2, ..., N_\mathrm{v}, \tag{7a}$$

$$\mathbf{T}(\mathbf{x}^c) = \sum_{v=1, v\neq c}^{N_\mathrm{v}} \mathbf{H}^\tau(\mathbf{x}^c, \mathbf{x}^v, \omega)\mathbf{S}^v + \mathbf{H}^\tau_{\mathrm{cc}}\mathbf{S}^c, \quad \text{for } c = 1, 2, ..., N_\mathrm{v}, \tag{7b}$$

where $\mathbf{H}_{\mathrm{cc}}$ and $\mathbf{H}^\tau_{\mathrm{cc}}$ represent the matrices of the OIFs associated with the Dirichlet and Neumann boundary conditions, respectively. Regarding the OIFs for the Neumann boundary condition, the fundamental solutions $\mathbf{H}^\tau(\mathbf{x}^c, \mathbf{x}^v, \omega)$ behaves as a singular function of the type $|\mathbf{x}^c - \mathbf{x}^v|^{-2}$ when $\mathbf{x}^c$ tends to $\mathbf{x}^v$ [48]. Thus, due to its hypersingular nature, its regularization has received particular interest in the literature. To derive these OIFs, a regularization strategy similar to the one used in standard BEM is considered. The procedure involves the application of the subtracting and adding-back technique in Eq. (7b) and using the rigid-body identity. This procedure is thoroughly explained in [45, 47] for the elastostatics and elastodynamic problems, respectively. Here, the formulation presented in [47] for determining the OIFs associated with the Neumann boundary condition is adopted. A three-dimensional version of that formulation results in

$$\mathbf{H}^\tau_{\mathrm{cc}} = \frac{1}{A^c}\left[\mathbf{I} + \mathbf{B}_{\mathrm{cc}} - \sum_{v=1, v\neq c}^{N_\mathrm{v}} A^v \mathbf{H}^\tau(\mathbf{x}^v, \mathbf{x}^c, 0)\right], \tag{8}$$

where the terms A^v and A^c represent the area of influence associated with the v-th and c-th sources, respectively, as shown in Fig. 3(c). $\mathbf{I}$ is the identity matrix, $\mathbf{H}^\tau(\mathbf{x}^v, \mathbf{x}^c, 0)$ is the matrix of static fundamental solutions for the tractions and $\mathbf{B}_{\mathrm{cc}}$ is given by

$$\mathbf{B}_{\mathrm{cc}} = \int_{\partial\Omega^c} \{\mathbf{H}^\tau(\mathbf{x}^c, \mathbf{x}, 0) - \mathbf{H}^\tau(\mathbf{x}, \mathbf{x}^c, 0)\}\, \mathrm{d}S_x, \tag{9}$$

where $\mathrm{d}S_x$ is a differential of area along the boundary portion $\partial\Omega^c$, which is the portion of influence of the c-th source, with a total area of A^c. Note that the integration in Eq. (9) is performed componentwise (i.e. the integration is performed for each component of the matrix). For arbitrarily smooth boundaries, by assuming that the considered source point moves gradually close to the considered collocation point along a line segment, the term $\mathbf{B}_{\mathrm{cc}}$ becomes zero [51, 52]. For general boundaries, $\mathbf{B}_{\mathrm{cc}}$ is still regular and can be numerically integrated using standard Gaussian quadrature [45].

Regarding the OIFs for the Dirichlet boundary condition, the fundamental solution $\mathbf{H}(\mathbf{x}^c, \mathbf{x}^v, \omega)$ undergoes a singular of behaviour of the form $|\mathbf{x}^c - \mathbf{x}^v|^{-1}$ [48] when $\mathbf{x}^c$ tends to $\mathbf{x}^v$. In this case, the associated OIFs $\mathbf{H}_{\mathrm{cc}}$ can be directly computed by averaging the fundamental solution over the boundary portion of influence where the virtual source is applied [45, 47, 52].

The linear systems of equations associated with Eqs. (7a) and (7b) can be written in matrix form as

$$\mathbf{U}_\mathrm{b} = \mathbf{H}_\mathrm{bb}\mathbf{S}, \quad \mathbf{T}_\mathrm{b} = \mathbf{H}^\tau_\mathrm{bb}\mathbf{S}, \tag{10}$$

where $\mathbf{U}_\mathrm{b}$, $\mathbf{T}_\mathrm{b}$ are the vectors that contain the three components of the displacements and tractions, respectively, at the boundary for all collocation points. The vector $\mathbf{S}$ contains the source intensities of all virtual sources and $\mathbf{H}_\mathrm{bb}$ and $\mathbf{H}^\tau_\mathrm{bb}$ are the corresponding matrices of frequency response functions of the soil for the displacement and traction, respectively. A unit vector normal to the boundary pointing outwards to the soil medium is considered when constructing $\mathbf{H}^\tau_\mathrm{bb}$. In a similar way, displacements $\mathbf{U}_\mathrm{s}$ at an arbitrary point in the soil medium can be computed using the matrix form of Eq. (7a), which can be written as

$$\mathbf{U}_\mathrm{s} = \mathbf{H}_\mathrm{sb}\mathbf{S}, \tag{11}$$

where $\mathbf{H}_\mathrm{sb}$ is the frequency response function matrix that relates the set of forces $\mathbf{S}$ with the responses at the particular arbitrary point.

2.3. Pile-soil coupling formulation

The pile-soil dynamic coupling is carried out by employing the dynamic substructuring technique considering the two subsystems presented in the previous two subsections, the pile and the soil with the pile's cavity inclusion. When coupling two elastic solids, this technique enforces compatibility of the strain and stress fields at their interface. In the proposed method for pile-soil problems presented in this work, these conditions are met by ensuring displacement and interaction forces compatibility at a set of collocation points distributed along the pile-soil interface. Interaction forces seen by the cavity at the collocation points are determined considering a constant distribution of the traction field in the vicinity of each particular collocation point, whilst these forces are transferred to the pile as point forces.

A detailed description of the collocation point distribution employed is presented in Fig. 4(a). A uniformly distributed set of N_p ring-shaped distributions of collocation points are deployed along the lateral pile-soil interface. Each ring-shaped distribution has a total of N_s uniformly distributed collocation points. Also, an additional collocation point is located at its centre in the bottom circular pile-soil interface. Therefore, this implies that the dynamic fields at the pile-soil interface are represented at $N_\mathrm{c} = N_\mathrm{s}N_\mathrm{p} + 1$ collocation points. As also shown in Fig. 4(a), a set of uniformly distributed pile centroid points constitutes the discretization scheme for the pile. Each of them is associated with a pile segment and also with a ring of collocation points. Based on the assumption that each of these pile segments is rigid, the corresponding responses at the collocation points at the pile-soil interface can be linked with the responses

of the pile at the centroid points. The derivation of this relation is presented in this section. Additionally, the areas of influence associated with each collocation point have been also depicted in Fig. 4(b). These areas are important in the application of the SBM to model the soil, as described in the previous section, as well as for the determination of the interaction forces applied to the pile from the tractions at the pile-soil interface.

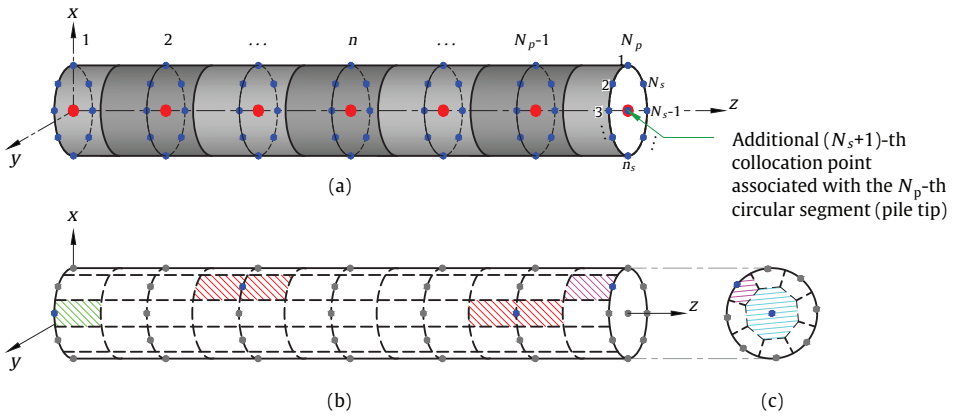

Figure 4: Discretization schemes adopted in this work (illustrated horizontally for convenience). In (a), the distribution of collocation points (blue dots) over the pile-soil interface, together with the corresponding pile centroid points (red dots) is displayed. In (b) and (c), the four distinct types of areas of influence are presented: In green, the area of influence of a collocation point located at the ground surface is shown; in red, the one for a collocation point located in an intermediate position along the lateral interface is illustrated; in magenta, the influence area for one point of the ring-shaped distribution at the pile tip is represented; and finally, in cyan, the area of influence of the collocation point located at the centre of the bottom pile-soil interface is displayed.

The displacements at all collocation points along the pile-soil interface are collected by the vectors $\mathbf{U}_b^s$ and $\mathbf{U}_b^p$ for the soil and pile subsystems, respectively. Displacement compatibility at the interface leads to $\mathbf{U}_b^s = \mathbf{U}_b^p$. Due to the assumption that each pile segment acts as a rigid body, the displacements $\mathbf{U}_b^p$ can be expressed in terms of the rigid body translation and rotation of the cylindrical segments defined at the corresponding pile centroid points displacements as

$$\mathbf{U}_b^p = \mathbf{W}\mathbf{U}_p, \tag{12}$$

where the $\mathbf{U}_p$ vector collects the displacements and rotations at all pile centroid points, and $\mathbf{W}$ is the transformation matrix that relates the six degrees of freedom of all pile centroid points with the three-component motion of all collocation points. Details of this transformation and the definition of $\mathbf{W}$ are given in Appendix B. The compatibility of the reaction forces at the interface is expressed as $\mathbf{P}_b^s = -\mathbf{P}_b^p$, with $\mathbf{P}_b^s$ and $\mathbf{P}_b^p$ being the interaction forces to which the soil and the pile are subjected, respectively, at all collocation points. As mentioned above, the present methodology assumes that the traction field in the pile-soil interface is constant along each influence area and equal to the value evaluated at its corresponding collocation point. Thus, the interaction forces to which the soil is subjected are given

by

$$\mathbf{P}_{\mathrm{b}}^{\mathrm{s}} = \mathbf{W}_{\mathrm{A}} \mathbf{T}_{\mathrm{b}}^{\mathrm{s}}, \tag{13}$$

where $\mathbf{W}_{\mathrm{A}}$ is a diagonal matrix that contains the areas of influence associated with all collocation points and $\mathbf{T}_{\mathrm{b}}^{\mathrm{s}}$ is the vector that contains the tractions at all collocation points along the pile-soil interface. Regarding the pile interaction forces, their summation for each pile segment results in equivalent three-component forces and moments applied to the corresponding pile centroid point. This transformation is analogous to the one presented for the translational and rotational motions: $\mathbf{P}_{\mathrm{p}} = -\mathbf{W}^{\mathrm{T}} \mathbf{P}_{\mathrm{b}}^{\mathrm{s}}$ (see Appendix B for more details). Thus, tractions at the pile-soil interface are related with the interaction forces and moments at the pile centroid as

$$\mathbf{P}_{\mathrm{p}} = -\mathbf{W}^{\mathrm{T}} \mathbf{W}_{\mathrm{A}} \mathbf{T}_{\mathrm{b}}^{\mathrm{s}}. \tag{14}$$

As discussed above, the transformations of motions and forces from the pile centroid points to the collocation points consider both translational and rotational motions, as well as forces and moments. A simplified approach has been taken into consideration in previous works about dynamic pile-soil interaction, for which the rotations and the moments are neglected within the coupling procedure. This assumption can also be applied in the context of the present formulation, as discussed in Appendix B. The efficiency and accuracy of such simplification are studied in Section 3.

The system is considered to be subjected to external forces at the pile head and at an arbitrary point in the soil, represented by the three-component vectors $\mathbf{F}_{\mathrm{p}}$ and $\mathbf{F}_{\mathrm{s}}$, respectively. Based on the superposition principle, the dynamic unknown states of the soil can be written as the summation of the motion induced by the external load $\mathbf{F}_{\mathrm{s}}$ and the motion induced by the traction boundary condition at the pile-soil interface. Thus, based on Eqs. (10) and (11), the response at the collocation points $\mathbf{U}_{\mathrm{b}}^{\mathrm{s}}$ and at an arbitrary point in the soil $\mathbf{U}_{\mathrm{s}}$ can be written as

$$\mathbf{U}_{\mathrm{b}}^{\mathrm{s}} = \mathbf{H}_{\mathrm{bb}} (\mathbf{H}_{\mathrm{bb}}^{\tau})^{-1} \mathbf{T}_{\mathrm{b}}^{\mathrm{s}} + \mathbf{H}_{\mathrm{bf}}^{\mathrm{cav}} \mathbf{F}_{\mathrm{s}}, \tag{15a}$$

$$\mathbf{U}_{\mathrm{s}} = \mathbf{H}_{\mathrm{sb}} (\mathbf{H}_{\mathrm{bb}}^{\tau})^{-1} \mathbf{T}_{\mathrm{b}}^{\mathrm{s}} + \mathbf{H}_{\mathrm{sf}}^{\mathrm{cav}} \mathbf{F}_{\mathrm{s}}, \tag{15b}$$

with $\mathbf{H}_{\mathrm{bf}}^{\mathrm{cav}}$ and $\mathbf{H}_{\mathrm{sf}}^{\mathrm{cav}}$ the receptance matrices relating the response at the collocation points and at that arbitrary point in the soil subsystem, respectively, due to the external force $\mathbf{F}_{\mathrm{s}}$. The superindex cav is used to denote that these receptance matrices of the soil should be determined by accounting for the inclusion of the cavity. They can be expressed in terms of the Green's functions of an elastic half-space with no inclusions as

$$\mathbf{H}_{\mathrm{bf}}^{\mathrm{cav}} = \mathbf{H}_{\mathrm{bf}} - \mathbf{H}_{\mathrm{bb}} (\mathbf{H}_{\mathrm{bb}}^{\tau})^{-1} \mathbf{H}_{\mathrm{bf}}^{\tau} \quad \text{and} \quad \mathbf{H}_{\mathrm{sf}}^{\mathrm{cav}} = \mathbf{H}_{\mathrm{sf}} - \mathbf{H}_{\mathrm{sb}} (\mathbf{H}_{\mathrm{bb}}^{\tau})^{-1} \mathbf{H}_{\mathrm{bf}}^{\tau}, \tag{16}$$

where the matrices $\mathbf{H}_{bf}$ and $\mathbf{H}_{sf}$ contain the Green's functions associated with the source point of $\mathbf{F}_s$ and the receivers at the collocation points or at the arbitrary point in the soil where $\mathbf{U}_s$ is to be determined, respectively. The matrix $\mathbf{H}^{\tau}_{bf}$ is analogous to $\mathbf{H}_{bf}$ but for traction response. In the expressions in Eq. (16) the second term of the right-hand side simulates the existence of the cavity by enforcing a traction-free field along the surface where the pile-soil interface should be.

Similar expressions can be derived for the pile subsystem, for which its responses at the collocation points $\mathbf{U}^{p}_{b}$ and at the pile head $\mathbf{U}_h$ are given by

$$\mathbf{U}^{p}_{b} = \mathbf{W}\left(\mathbf{H}_{ph}\mathbf{F}_p - \mathbf{H}_{pp}\mathbf{W}^{T}\mathbf{W}_A\mathbf{T}^{s}_{b}\right), \tag{17a}$$

$$\mathbf{U}_h = \mathbf{H}_{hh}\mathbf{F}_p - \mathbf{H}_{hp}\mathbf{W}^{T}\mathbf{W}_A\mathbf{T}^{s}_{b}, \tag{17b}$$

in which $\mathbf{H}_{ph}$, $\mathbf{H}_{pp}$, $\mathbf{H}_{hh}$ and $\mathbf{H}_{hp}$ are the matrices of receptance functions that relate the response at all pile centroid points or at the pile head (represented by p and h, respectively, as the first subscript) due to forces along the pile or at the pile head (represented by the same nomenclature for the second subscript).

By applying the compatibility of displacements and using Eqs. (15a) and (17a), the tractions at the pile-soil interface can be determined and subsequently substituted to Eqs. (15b) and (17b) to find the final expressions for the coupled pile-soil system which allow for calculating the responses of an arbitrary point in the soil or the pile head, respectively. These responses of the coupled system can be written as a function of the external loads as

$$\mathbf{U}_s = \mathbf{H}^{c}_{sh}\mathbf{F}_p + \mathbf{H}^{c}_{sf}\mathbf{F}_s, \tag{18a}$$

$$\mathbf{U}_h = \mathbf{H}^{c}_{hh}\mathbf{F}_p + \mathbf{H}^{c}_{hf}\mathbf{F}_s, \tag{18b}$$

where $\mathbf{H}^{c}_{sh}$, $\mathbf{H}^{c}_{sf}$, $\mathbf{H}^{c}_{hh}$ and $\mathbf{H}^{c}_{hf}$ are the receptance matrices of the coupled system that provide the relationship between the response of an arbitrary point in the soil or the pile head (identified in the first subscript by s and h, respectively) due to forces applied to the soil at another arbitrary point or forces applied to the pile head (identified by the second subscripts f and h, respectively). These matrices are given by the following expressions

$$\mathbf{H}^{c}_{sh} = \mathbf{H}_{sb}(\mathbf{H}^{\tau}_{bb})^{-1}\boldsymbol{\Upsilon}\mathbf{W}\mathbf{H}_{ph}, \tag{19a}$$

$$\mathbf{H}^{c}_{sf} = \mathbf{H}^{cav}_{sf} - \mathbf{H}_{sb}(\mathbf{H}^{\tau}_{bb})^{-1}\boldsymbol{\Upsilon}\mathbf{H}^{cav}_{bf}, \tag{19b}$$

$$\mathbf{H}^{c}_{hh} = \mathbf{H}_{hh} - \mathbf{H}_{hp}\mathbf{W}^{T}\mathbf{W}_A\boldsymbol{\Upsilon}\mathbf{W}\mathbf{H}_{ph}, \tag{19c}$$

$$\mathbf{H}^{c}_{hf} = \mathbf{H}_{hp}\mathbf{W}^{T}\mathbf{W}_A\boldsymbol{\Upsilon}\mathbf{H}^{cav}_{bf}, \tag{19d}$$

with

$$\Upsilon = \left[\mathbf{H}_{\mathrm{bb}}(\mathbf{H}_{\mathrm{bb}}^{r})^{-1} + \mathbf{W}\mathbf{H}_{\mathrm{pp}}\mathbf{W}^{\mathrm{T}}\mathbf{W}_{A}\right]^{-1}. \tag{20}$$

Eqs. (18a) and (18b) inherently contain the solution to both radiation and scattering problems for the system under study, which can be extracted by enforcing $\mathbf{F}_{\mathrm{s}} = \mathbf{0}$ or $\mathbf{F}_{\mathrm{p}} = \mathbf{0}$, respectively.

Finally, note that the formulation of the proposed model is not limited to single piles and/or homogeneous soils. While the case of a multi-pile foundation can be directly considered by considering displacement compatibility and force equilibrium on each pile, considering horizontally layered soils instead of homogeneous ones only requires using the corresponding Green's functions in the calculation.

3. Numerical assessment of the proposed approach

A numerical assessment of the proposed approach is presented in this section. For this purpose, a convergence study is initially performed to define suitable values for N_{p} and N_{s} that ensure an acceptable degree of convergence that allows for defining a general criterion to select the number of collocation points required for a specific problem. Although the study presented in Section 3.1 only focuses on the convergence of the method itself, it is worth mentioning that the accuracy of the converged results has also been verified for each one of the calculation cases considered. The accuracy of the proposed method is discussed in detail in Section 3.2 in which the method is compared with other existing state-of-the-art methodologies. The aim is to demonstrate the accuracy of the method and discuss its numerical efficiency in the framework of two problems: the radiation problem, for which the response of the pile-soil system due to the force $\mathbf{F}_{\mathrm{p}}$ on the pile is calculated; and the scattering problem, in which the system response to a load $\mathbf{F}_{\mathrm{s}}$ on the soil is evaluated. These numerical studies are performed in the context of three different pile-soil systems: a short pile embedded in soft soil (Case 1); a short pile embedded in stiff soil (Case 2); and a long pile embedded in soft soil (Case 3). The soil is modelled as a homogeneous elastic half-space for all these cases.

The specific geometrical and mechanical parameters considered for the three cases are presented in Table 1. The dimensions of the piles and the soil properties have been selected to assess the performance of the proposed methodology in very different situations rather than attempting to represent realistic scenarios. Therefore, while the pile aspect ratio of the short pile case ($L_p/r_p = 33.4$) is similar to those considered in other works in the field [42, 53], the long pile $L_p/r_p = 100$ has been chosen to assess the performance of the method for a very slender pile. The material damping is introduced in the soil by considering complex Lamé constants λ^* and ν^* given by $\lambda^* + 2\nu^* = (\lambda + 2\nu)(1 + \mathrm{i}2D)$ and $\nu^* = \nu(1 + \mathrm{i}2D)$ for positive-valued frequencies, where D represents the hysteretic material damping ratio of the soil. The frequency range of interest is selected to be $1 - 100$ Hz in accordance with the frequency range in which ground-borne vibration is typically significant [54]. For the comparison of results,

three observation points are considered: O_1, O_2 and O_3, located at positions $(0,0,0)$, $(5,0,0)$ m and $(20,0,0)$ m, respectively; the first one is collecting the pile head response and the other two are collecting the response of the soil surface at the near and far field. Furthermore, the results are presented in terms of magnitude of the free-field and pile-head frequency response functions receptances in dB with 1 m/N as reference. This form of presentation is particularly adequate to compare the performance of various numerical models, as it does not involve any additional assumption or source of inaccuracy, such as the ones that could arise when dynamic stiffness results are normalised by their static counterparts [21]. Moreover, as the free-field and pile-head responses depend on the pile-soil interaction forces, the obtention of accurate results strongly suggests that the model adequately captures any dynamic unknown state at the pile-soil boundary.

Description	**Units**	**Soft soil**	**Stiff soil**	**Short pile**	**Long pile**
Density (ρ)	kg/m^3	1950	2000	2860	2860
Young' modulus (E)	MPa	151.2	445.5	40000	40000
Poisson's ratio (ν)	-	0.35	0.40	0.25	0.25
Hysteretic damping ratio (D)	-	0.05	0.02	0.01	0.01
Speed of the P-waves (C_p)	m/s	352.8	703.6	-	-
Speed of the S-waves (C_s)	m/s	169.5	287.2	-	-
Pile length (L_p)	m	-	-	10	35
Pile radius (r_p)	m	-	-	0.3	0.35

Table 1: Pile and soil parameters used in the considered numerical examples.

Regarding the computation details, the elastic half-space Green's functions required in the proposed approach as well as for the 3D FE-BE approach employed for verification purposes, are computed with the EDT toolbox [55]. Algorithms for all methods have been implemented in MATLAB, and the simulations have been carried out on a 40-core high-performance cluster with 2 GHz Intel® Xeon® Gold 6138 CPU.

Finally, the term $\mathbf{B}_{\mathrm{cc}}$ presented in Eq. (9) has been neglected from the calculations to enhance thus the computational efficiency of the proposed method since, as discussed in Section 2.2 and reported in [47, 51, 52], this term has almost no impact on the accuracy of the results in the case of smooth boundaries. This fact has been also verified numerically for each one of the considered examples; however, a detailed analysis of the importance of this term for arbitrarily shaped cavities is beyond the scope of this work and will be addressed in future studies

3.1. Convergence analysis of the semi-analytical approach

This subsection aims to provide a criterion for defining N_p and N_s values that ensure an acceptable trade-off between accuracy and numerical performance. In the context of the BEM, it is usually stated that element size should be between six and ten times smaller than the minimum wavelength of the problem [56]. This statement may not be representative of the SBM, taking into account the meshless nature of the method. In this sense, a convergence study

to determine appropriate N_p and N_s values is presented in this section. For this analysis, only the radiation problem for the Case 1 is presented; however, similar results have been derived for the other two cases (not included here). The response of this case has been computed for values of N_p ranging between 5 and 60, and for N_s between 4 and 40. The excitation frequency is set to the maximum of the frequency range, being 100 Hz. The convergence analysis is performed by comparing the results obtained for the different values of N_p and N_s with those obtained for a reference case with $N_\mathrm{p}^\mathrm{ref} = 70$ and $N_\mathrm{s}^\mathrm{ref} = 40$. The discrepancies between each case and the reference one are presented in terms of a relative error, which is given by

$$\varepsilon_{ij} = \frac{\left| H_{k\mathrm{h}}^{\mathrm{c},ij} - H_{k\mathrm{h,ref}}^{\mathrm{c},ij} \right|}{\left| H_{k\mathrm{h,ref}}^{\mathrm{c},ij} \right|}, \tag{21}$$

where ε_{ij} is the relative error of the receptance component $H_{k\mathrm{h}}^{\mathrm{c},ij}$ with respect to the reference one $H_{k\mathrm{h,ref}}^{\mathrm{c},ij}$. The first superscript i denotes the response direction, while j is referred to the force direction. The subscript k is defined as $k = \mathrm{h}$ or $k = \mathrm{s}$ according to whether the response is evaluated on the pile head or at the ground surface, respectively.

Fig. 5 shows the convergence analysis results at the three observation points. For clarity, the results are presented in logarithmic scale. As expected, the relative errors decrease as the values of N_p and N_s increase. Very small relative errors are observed for values of N_p and N_s above 50 and 18, respectively, suggesting that the results of the proposed method have numerically converged. The vertical driving-point response at the pile head (associated with ε_{zz}) in Figs. 5(a-i), 5(b-i) and 5(c-i) converges for smaller values of N_p and N_s than the lateral driving-point response (associated with ε_{xx}, ε_{yy}). Moreover, the lateral driving-point responses are more sensitive with respect to N_s than the vertical driving-point responses, which are almost insensitive to changes in N_s. These trends are less prominent for soil response.

The convergence analysis shows that discrepancies smaller than the difference between the reference results and the results obtained when considering at least eight collocation points per wavelength in the longitudinal direction are below -1.25 in the logarithmic scale used in Fig. 5, which corresponds to differences below 0.2 dB with respect to the reference solution. Thus, N_p is suggested to be defined based on this criterion. For the specific problem under investigation, where the minimum wavelength is $\lambda_\mathrm{min} = 1.695$ m, this criterion indicates that N_p should be at least 47 (see vertical dashed green lines in Fig. 5). Regarding the discretization scheme for the collocation points within the ring-shaped distributions along the perimeter of the pile segments, the convergence study demonstrated that a practical rule for defining an appropriate value for N_s is $N_\mathrm{s} \geqslant 32\pi r_\mathrm{p}/\lambda_\mathrm{min}$, in which λ_min stands for the minimum wavelength of the problem. Consequently, the minimum number of collocation points per wavelength along each ring-shaped distribution is 16. This rule is especially important to be complied when the lateral driving-point response at the pile head is computed. Following this criterion, the suggested value for N_s is 18 (see horizontal dashed green

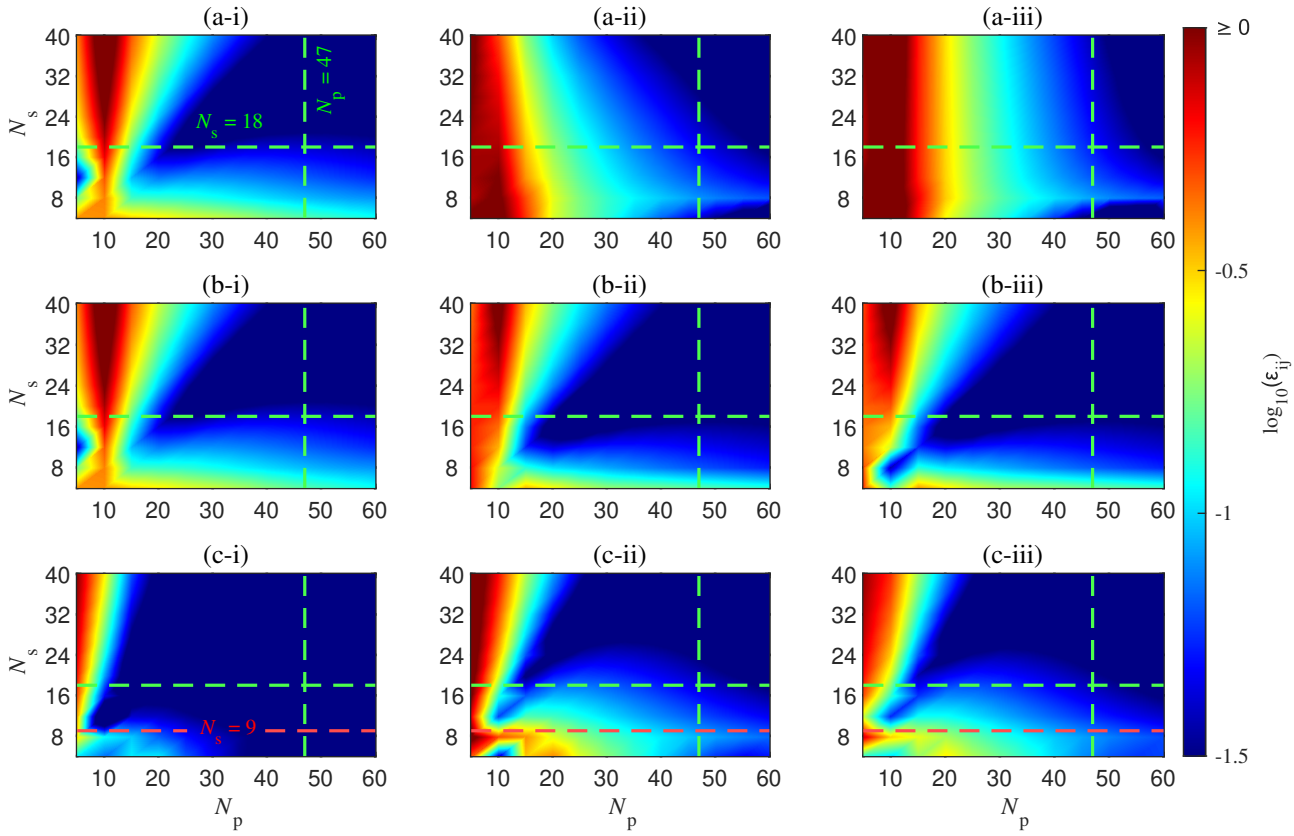

Figure 5: Relative errors (depicted in logarithmic scale) ε_{xx} (a), ε_{yy} (b) and ε_{zz} (c) associated with the response at the observation points O_1 (i), O_2 (ii), O_3 (iii), respectively, for the case of a short pile embedded in soft soil.

lines in Fig. 5). When only the vertical response due to vertical loading is computed, this criterion can be significantly relaxed and a value $N_s \geqslant 16\pi r_p/\lambda_{min}$ is found to be working well in this situation. For the specific problem under investigation, the N_s value suggested for computing ε_{zz} is 9, (see horizontal dashed red lines in Fig. 5(c-i), (c-ii) and (c-iii)).

Furthermore, the efficacy of the proposed discretization rules has been studied by comparing the results for four discretization schemes, which are: $N_p = 70$ and $N_s = 40$; $N_p = 50$ and $N_s = 32$; $N_p = 35$ and $N_s = 8$; and $N_p = 15$, $N_s = 8$. The resulting frequency response functions (FRFs) are presented in Fig. 6 and show that, as suggested by the relative error results, there is almost no difference between the cases that consider N_p and N_s values that comply with the previously stated criteria. It should be noticed that, as shown by the relative errors, vertical responses due to a vertical load on the pile head are predicted with reasonable accuracy by the proposed approach, even for low N_p and N_s values, as shown in Fig. 6(c-i), (c-ii) and (c-iii), where differences of less than 1 dB are found, occurring at 100 Hz. On the contrary, the responses related to lateral motions and/or loading are more sensitive to such changes.

The proposed criterion for defining the N_s and N_p values has been tested in other scenarios proving its correctness in all those situations. The mechanical and geometry parameters employed for testing these criteria ranged between the ones described for piled foundation Case 1 and Case 3. Therefore, for the sake of brevity, only the convergence analysis for the case associated with the minimum wave speed (Case 1) is shown since it is the one requiring the highest density of collocation and source points.

3.2. Comparison with existing approaches

In this section, the proposed modelling approach is compared with other well-established approaches in terms of its accuracy. This study serves to verify the approach and to test the discretization criteria discussed in the previous section. Furthermore, the need to account for rotational motion and torques when coupling both pile and soil subsystems has been also assessed. This study is performed for the radiation problem of Case 1, Case 2 and Case 3 scenarios.

The methods considered for comparison in this validation study are Novak's approach [2]; an axisymmetric FE-based approach that uses perfectly matched layers (PML) to avoid wave reflections at the borders of the model referred to as aFE-PML [34]; and a 3D FE-BE approach consisting of a 3D BE-based approach developed on the basis of [48]. Table 2 summarises the discretization schemes adopted for the proposed method, the aFE-PML and the FE-BE methodologies, particularly defining the number of nodes per wavelength (NPW) considered and the resulting discretization or mesh parameters. Additionally, Table 3 provides the number of collocation points or nodes, as well as the number of elements N_E, used in the different numerical models considered in this study. The 3D FE-BE approach has been implemented using four-noded quadrilateral BEs and eight-noded hexahedral FEs, whilst the aFE-PML method uses six-noded triangular elements to construct its meshes.

Although a detailed description of the aFE-PML approach is not in the scope of the present paper, it is worth mentioning some general information about the PML formulation. For the three pile cases computed with the aFE-PML approach, a stretching function with a constant value of 20 for the attenuation function is considered, as suggested in [57, 58], the thickness of the PML layer has been set to be 1 m in the radial and vertical direction, dividing the layer into six sub-layers. Regarding Novak's approach, the soil lateral reaction equation described in [2] does not correspond to the one proposed by Baranov in his original work [4]. This imprecise transcription of the original Baranov's formula could lead to inaccurate results for lateral driving-point responses. Corrected closed-form expressions for the soil reaction, originally proposed by Baranov, have been revisited in Appendix C. Additionally, the equation for obtaining the lateral response of the pile proposed in [2], which considers either the pile with both ends fixed or the pile head fixed and the pile tip pinned, is adapted to the case where both ends are free.

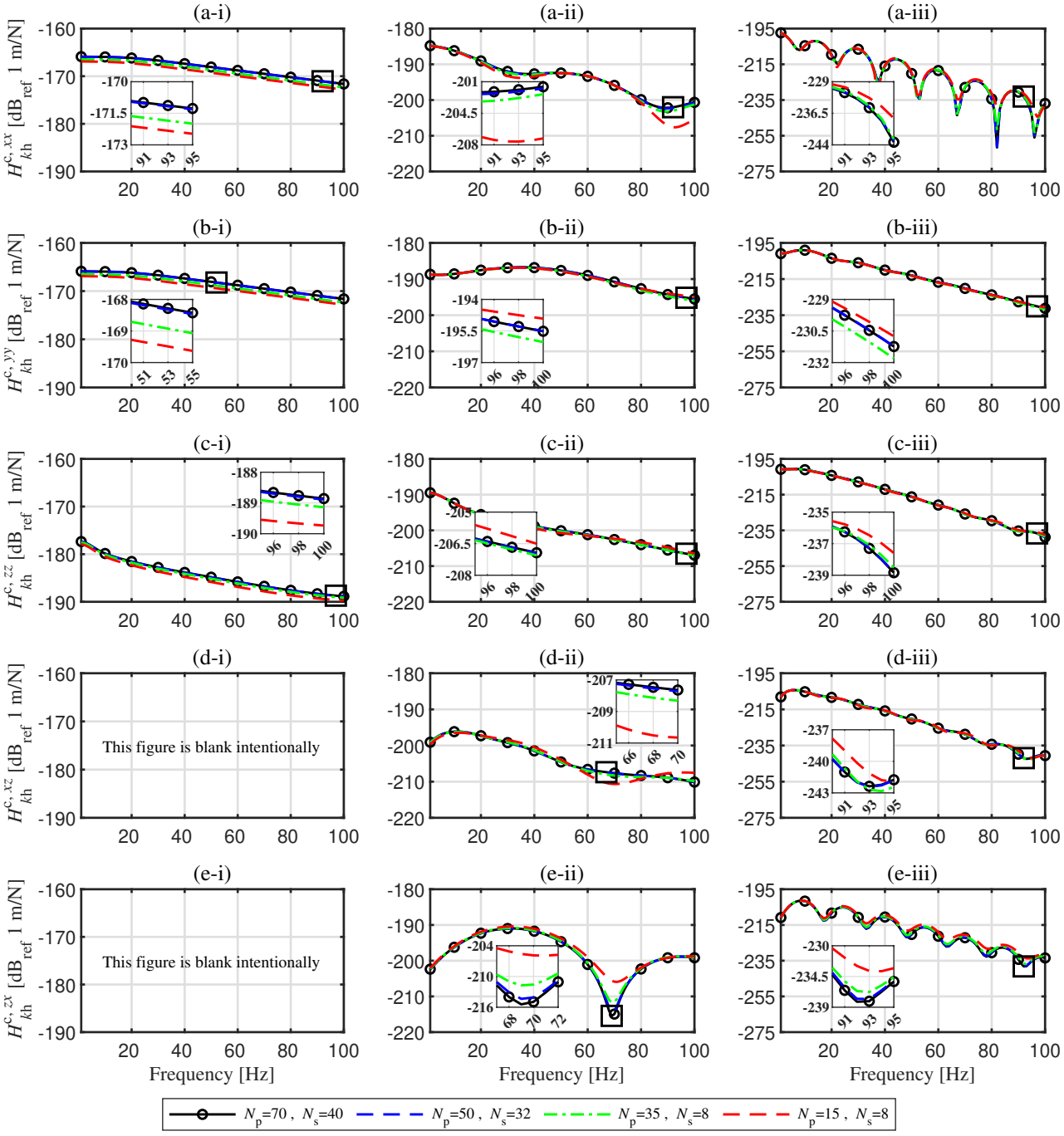

Figure 6: Displacement FRFs (receptances) for the radiation problem in the context of Case 1 scenario considering different discretization schemes. Components of the FRFs matrices shown are xx (a), yy (b), zz (c), xz (d) and zx (e) and observation points considered are O_1 (i), O_2 (ii), O_3 (iii). Results in dB using $20\log_{10}(|H|)$, with 1 m/N as reference.

Although Novak's approach is generally a suitable and extremely efficient approach for modelling pile driving cases, the method does not perform well at low frequencies and cannot predict the free-field response. Additionally, due to its axisymmetric nature, the aFE-PML approach can only be used to predict the system's dynamic vertical and radial responses to vertical excitations applied on the pile axis. However, both methods are included in the comparison study to highlight the proposed method's potential and increase the validation process's merit. Regarding the latter, since the FE-BE model was developed within this study to validate the proposed method and assess its computational efficiency, it was also considered necessary to verify the FE-BE results by including the comparison against results from other available tools. It is worth mentioning that although there are several alternative pile-soil interaction models based on analytical elastic-continuum formulations to deal with single pile foundations [17–20], these models have not been considered in the presented comparisons since they involve assumptions that are not considered in the presented numerical approaches, as discussed in Section 1 and reported in [1].

Description	**Proposed approach**				**3D FE-BE**		**aFE-PML**	
Case study	NPW	d [cm]	N_p	N_s	NPW	d [cm]	NPW	d [cm]
Case 1: Short pile - soft soil	8	21	47	28	9	20	7	25
Case 2: Short pile - stiff soil	9	32	32	18	14	20	6	45
Case 3: Long pile - soft soil	8	21	165	32	4	50	7	25

Table 2: Discretization schemes adopted for the proposed 3D FE-BE and aFE-PML approaches. The variable d represents the distance between collocation points along the longitudinal direction of the pile in the proposed approach and the element size in the mesh-based approaches.

Description	**Proposed approach**	**3D FE-BE**				**aFE-PML**	
Case study	SB points	FE mesh		BE mesh		FE mesh	
	N_c	Nodes	N_E	N_c	N_E	Nodes	N_E
Case 1: Short pile - soft soil	1317	3723	3000	1273	1260	125685	62464
Case 2: Short pile - stiff soil	577	3723	3000	1273	1260	85890	42605
Case 3: Long pile - soft soil	5281	5183	4200	1740	1753	125685	62464

Table 3: Number of collocation points (or nodes) and elements used in the different numerical models considered in the numerical assessment.

Fig. 7 to Fig. 9 show the displacement FRF (receptance) at each one of the observation points to forces applied on the pile head obtained by the different approaches mentioned above. An alternative version of the proposed approach that does not account for rotations and torques in the coupling between the pile and the soil is also included in the comparison. It can be seen that the responses due to vertical loads simulated by all the considered methods demonstrate a good agreement between them. Some differences between the methods can be seen in the results of the responses due to lateral loading. This is particularly clear for the Novak approach, which is found to be inaccurate at low frequencies for the lateral driving-point responses. Results show that the Novak method underestimates the lateral stiffness of the pile in a range of frequencies that mainly depends on the mechanical properties of the soil rather than the pile geometry, having inaccurate results arising below 20 Hz for the soft soil cases and below 40 Hz in the stiff soil

case. On the contrary, a good agreement over the whole frequency range is observed when comparing the results of the proposed methodology with those obtained with the other two numerical approaches. The results also show that when rotations and bending moments are not included in the coupling procedure, the proposed methodology may predict inaccurate responses to lateral loads. This effect can be observed in Figs. 7 to 9, that show discrepancies between the two coupling assumptions for the x and z soil responses due to lateral forces in the x-direction, especially at high frequencies. However, the impact of neglecting rotations and bending effects is much smaller for the remaining lateral loading responses.

Overall, the results from the comparison study presented in this section demonstrate the high accuracy of the proposed approach due to the agreement of its corresponding results with the ones delivered by the 3D FE-BE methodology, which is expected to provide highly detailed results.

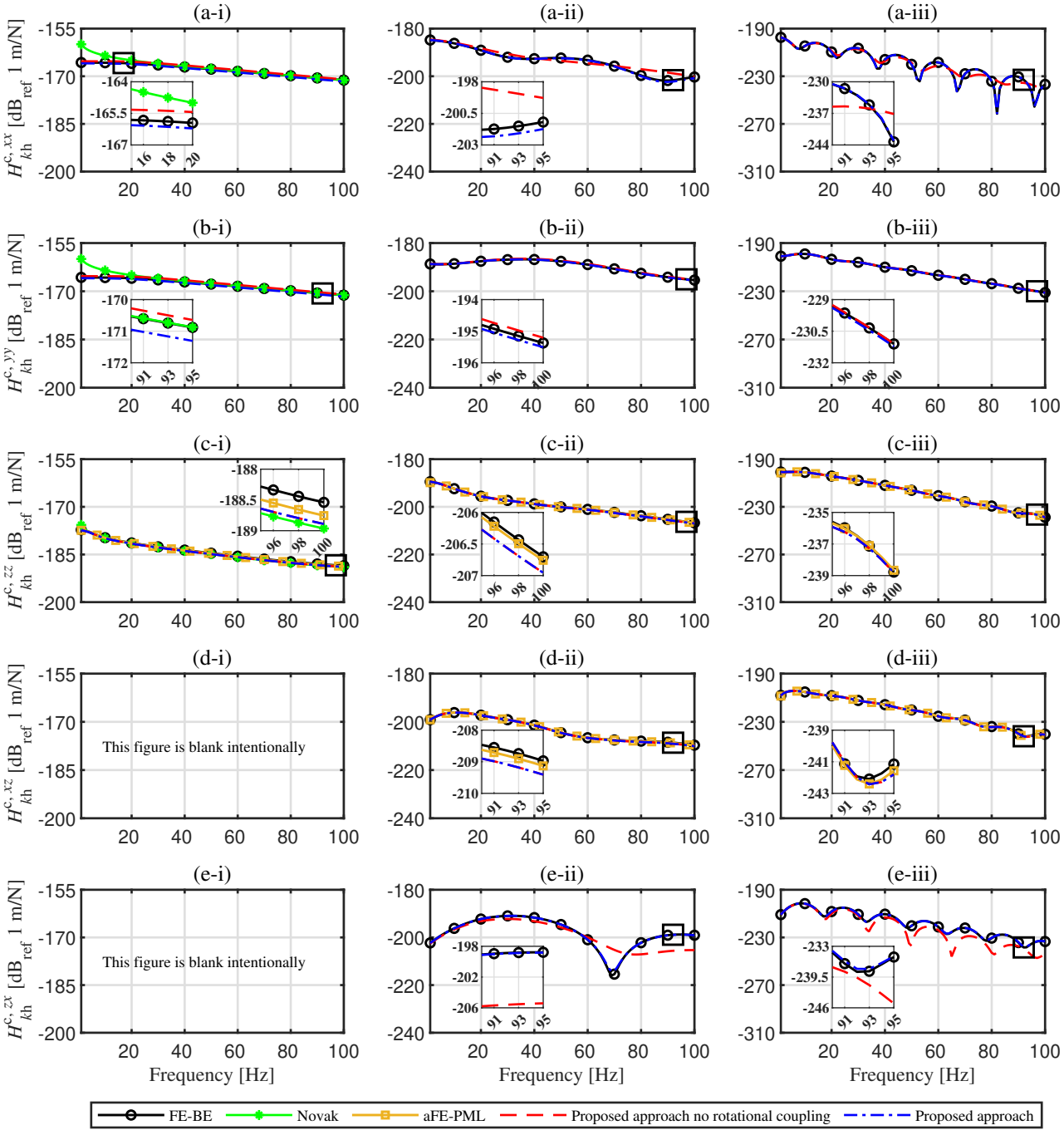

Figure 7: FRFs for the radiation problem in the framework of Case 1 (short pile & soft soil) scenario considering different approaches. Components of the FRFs matrices shown are *xx* (a), *yy* (b), *zz* (c), *xz* (d) and *zx* (e) and observation points considered are O_1 (i), O_2 (ii), O_3 (iii). Results in dB using $20\log_{10}(|H|)$, with 1 m/N as reference.

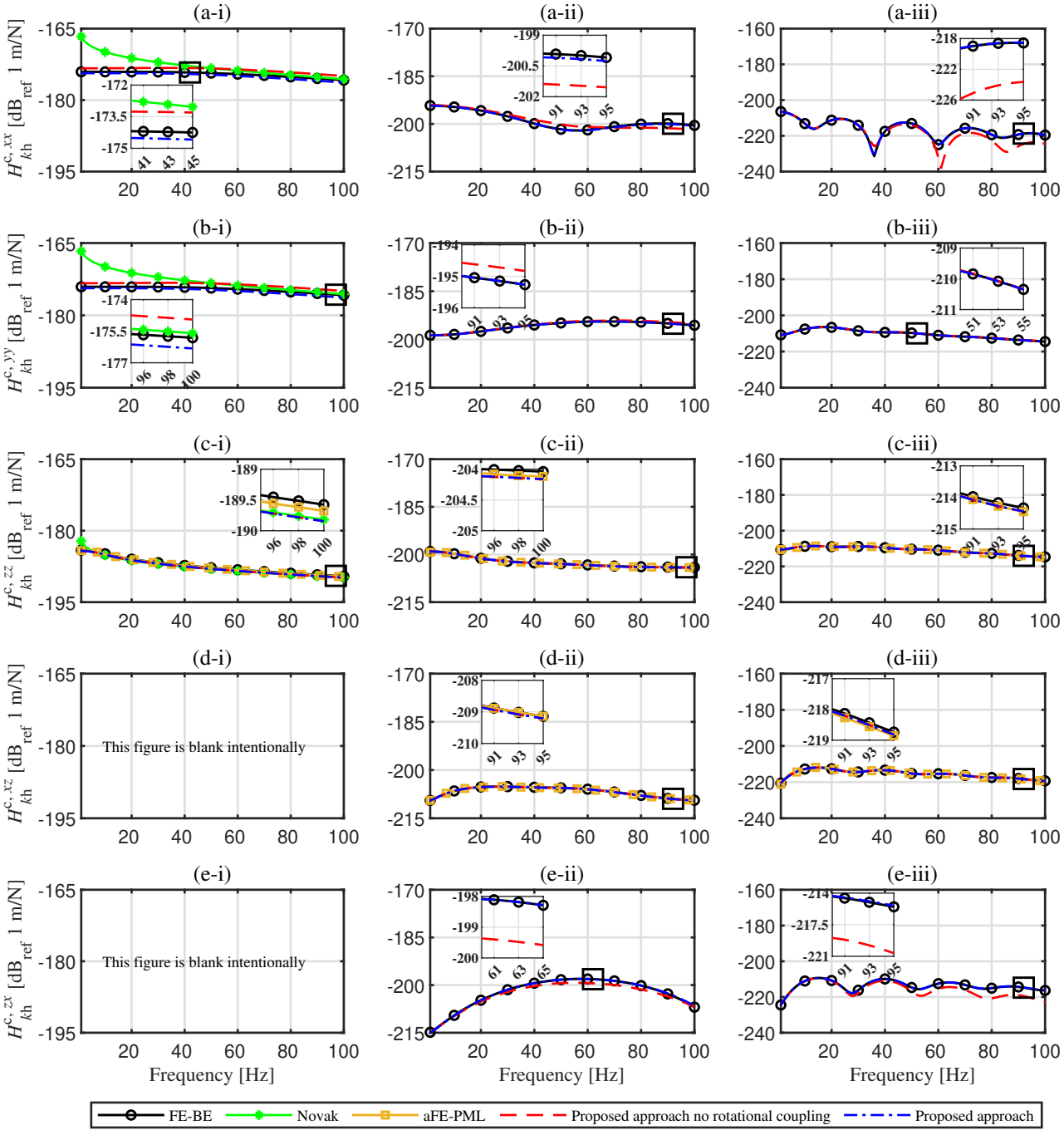

Figure 8: FRFs for the radiation problem in the framework of Case 2 (short pile & stiff soil) scenario considering different approaches. Components of the FRFs matrices shown are *xx* (a), *yy* (b), *zz* (c), *xz* (d) and *zx* (e) and observation points considered are O_1 (i), O_2 (ii), O_3 (iii). Results in dB using $20\log_{10}(|H|)$, with 1 m/N as reference.

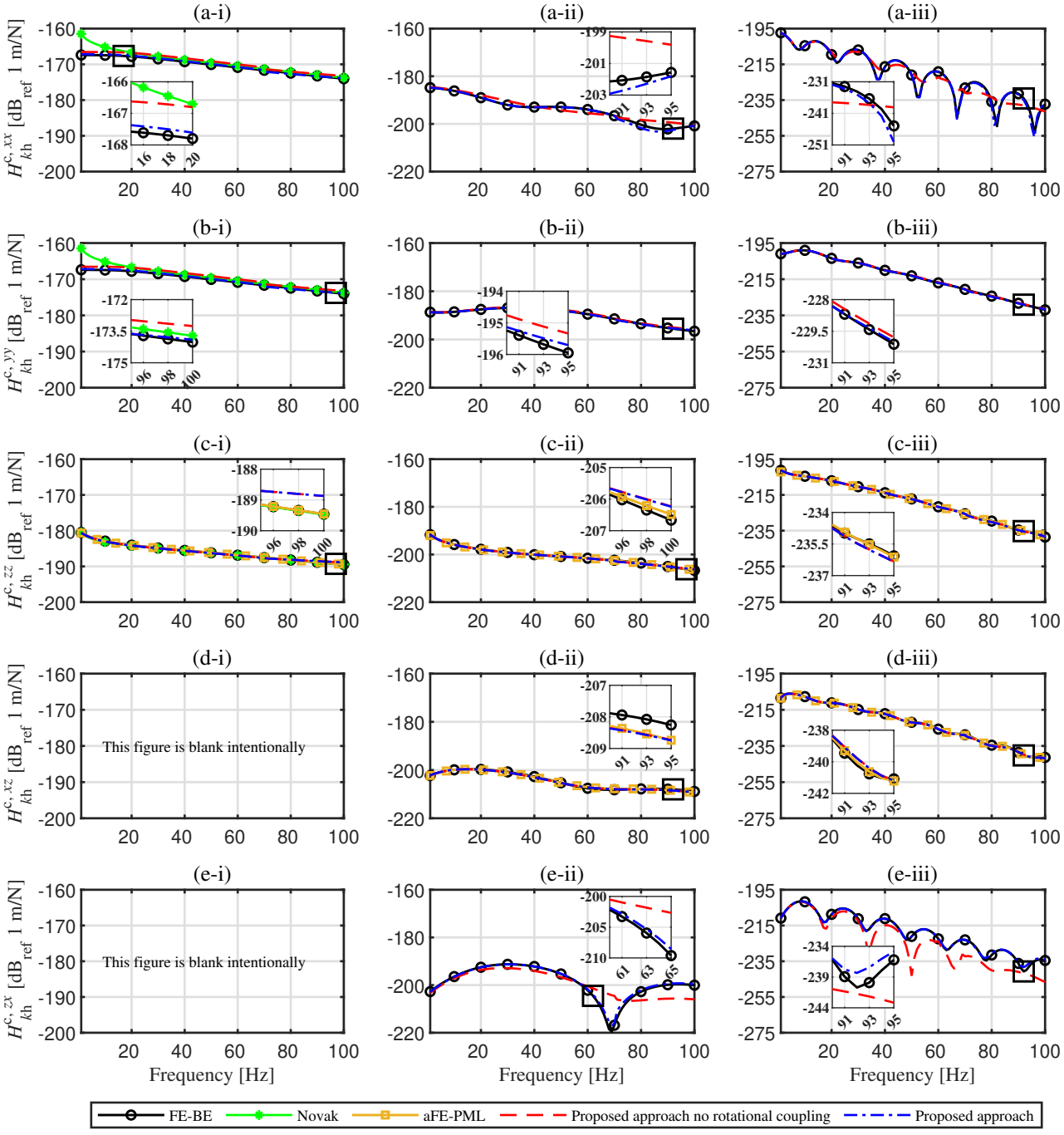

Figure 9: FRFs for the radiation problem in the framework of Case 3 (long pile & soft soil) scenario considering different approaches. Components of the FRFs matrices shown are *xx* (a), *yy* (b), *zz* (c), *xz* (d) and *zx* (e) and observation points considered are O_1 (i), O_2 (ii), O_3 (iii). Results in dB using $20\log_{10}(|H|)$, with 1 m/N as reference.

3.3. Verification of the dynamic reciprocity of the proposed approach

In the context of ground-borne vibration problems, the response of the pile due to a dynamic load applied on the ground is the most interesting problem to study since it allows for determining the response of buildings or structures with piled foundations to the action of incident elastic wave fields. This problem can be referred to as a scattering problem where, instead of determining the response of the soil, the vibration of the pile is what is required. However, employing the dynamic reciprocity theorem, this result can be obtained by solving the radiation problem for the case that the response is determined at the position where the load in the original scattering problem is intended to be placed.

In this section, a numerical study to verify that the proposed approach fulfils the dynamic reciprocity theorem is presented, which states the following property of the fundamental or Green's function of an elastic system as $\mathbf{H}(\mathbf{x}, \mathbf{y}, \omega) = \mathbf{H}^{\mathrm{T}}(\mathbf{y}, \mathbf{x}, \omega)$, which also applies for any FRF of the system. Due to the special assumptions taken into consideration in the proposed approach, it is worth checking the correctness for the proposed approach and for the alternative version that only considers translational coupling when dealing with the pile-soil interaction. Thus, the radiation problem of a force applied at the pile head and the response evaluated at the point O_2, governed by Eq. (19a), is compared to the scattering problem where the force is applied at the point O_2 and the response is evaluated at the pile head, governed by Eq. (19d). Results are shown in Fig. 10, from which it can be observed that the reciprocity for the proposed approach is satisfied. Therefore, it can be deduced that the dynamic reciprocity is fulfilled over the frequency range of interest in all situations for both studied coupling strategies employed within the proposed approach.

3.4. Summary of the computational efficiency of the proposed approach

In the cases studied in the previous subsections, it was shown that the proposed approach offers several advantages over the other methods. Compared with Novak's method, although significantly more computationally demanding, it can perform with better accuracy and include the results in the free field. Similarly, compared with the aFE-PML method, the proposed method overcomes the fundamental limitation on obtaining the results due to excitations at the free field (incident wave fields) and lateral excitations at the pile. Also, it avoids the high computational cost of dealing with far evaluation points and the requirements for a large mesh of the soil (a similar issue can be extrapolated for the 3D FE-PML model).

The 3D FE-BE methodology can provide accurate results in all directions; however, an inherent disadvantage of this method is associated with the computational effort. This is because the 3D FE-BE model requires a significant number of Green's function evaluations for solving the numerical integration over each of the BEs of the constructed

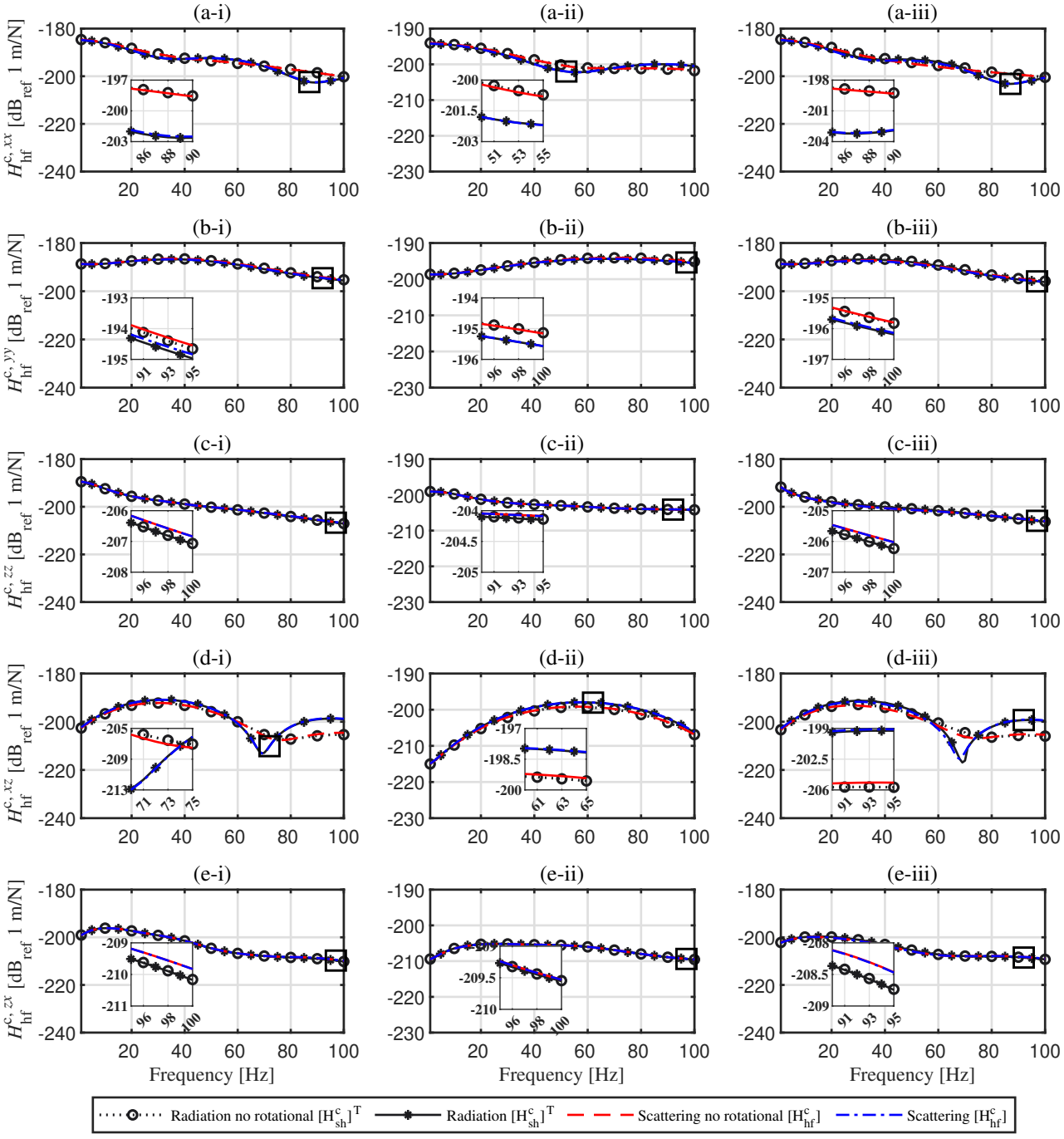

Figure 10: Response of the radiation and corresponding scattering problems in the context of the Case 1 (i), Case 2 (ii) and Case 3 (iii) scenarios. Components of the FRFs matrices shown are *xx* (a), *yy* (b), *zz* (c), *xz* (d) and *zx* (e). Results in dB using $20\log_{10}(|H|)$, with 1 m/N as reference.

mesh. This computational effort increases rapidly when the mesh density increases, either to fulfil high-frequency range requirements or to include multiple piles. The current work does not include a detailed computational efficiency

comparison, particularly against the FE-BE approach, because such an effort would depend (to some extent) on the programmer's skill in the computational implementation of the two methods. Furthermore, as described in Table 3, the SBM and BEM have modelled the pile cavity with different numbers and arrangements of collocation points so that a quantitative comparison of the computational times between them appears to be unfair. However, a general overview of the computational benefits of the SBM over the BEM is included here. Previous work in the fields of elastostatics [45] and acoustics [59] showed that the SBM can outperform the BEM in terms of accuracy when considering the same number of collocation points. Having that in mind, consider, for instance, a generic BE mesh consisting of N_{E} boundary elements and N_{c} collocation points and assuming a moderate number of Gaussian points $GP = 2 \times 2$ for a bilinear interpolation function of elements that are not severely distorted, as suggested in [48]. The BEM would require at least $n = GP \times N_{\mathrm{E}} \times N_{\mathrm{c}}$ Green's functions evaluations to obtain the unknown states of the system. In contrast, a corresponding SBM model considering the same number of collocation points would require $n = N_{\mathrm{c}}^2$ computations. Therefore, considering the BEM and SBM employing the same collocation point distribution to characterize the unknown states of the cavity, the inequality $N_{\mathrm{c}}^2 < GP \times N_{\mathrm{E}} \times N_{\mathrm{c}}$ holds and demonstrates the SBM to be more computationally efficient than the BEM, generally speaking. Moreover, although different numbers and arrangements of collocation points are employed to model the soil sub-system with the BEM and the SBM, the differences in computational requirements between these two approaches were observed when computing the results included in this paper. This difference was particularly significant for the pile foundation Case 3 when, even utilizing a discretization scheme incorporating six NPW, considerable computational efforts in terms of processor speed and rapid access memory was required for calculating the response of that pile-soil system. For these reasons, only four nodes per wavelength were employed in the modelling, as reported in Table 2, which has induced some inaccuracies at higher frequencies in the semi-analytical response, as shown in Fig. 9(a-ii), (a-iii), or (e-iii). Due to the meshless nature of the proposed approach, a significantly smaller number of Green's function evaluations are required to obtain the response of the targeted pile-soil system using the proposed method, resulting in a large reduction of the computation resources employed in the simulation.

4. Conclusions

A computationally efficient 3D approach for predicting pile-soil interaction problems is presented in this paper. The proposed method models the soil as a half-space and represents the pile as an Euler-Bernoulli beam to capture its flexural motion and as a rod to account for axial deformations. Regarding the coupling, the soil reaction is modelled using the SBM, an emerging meshless numerical method with computational efficiency and formulation simplicity merits exploited in the proposed scheme. The pile is divided into circular segments, each of them involving a set of

collocation points, placed at soil-pile interface, in which the compatibility of displacements and tractions between the two sub-systems is enforced. A transformation matrix is introduced to relate the pile response at the collocation points in the pile-soil interface with the pile response computed at the pile's centroid. This matrix is constructed assuming each pile segment to be rigid and considering both translational and rotational motions of the pile segments, as well as forces and bending moments.

The outcomes of the present work can be summarised in the following list of findings:

- The convergence analysis conducted for the proposed approach has provided a criterion for defining the number of pile segments and the number of collocation points per segment that ensures an acceptable trade-off between robustness, accuracy and numerical performance of the scheme.

- The proposed methodology has been verified against a 3D FE-BE methodology, an axisymmetric aFE-PML approach and compared with the Novak's method. Moreover, the reciprocity principle has been also verified for the proposed methodology in order to assess the correctness of the formulation presented. In the calculation examples considered, the method is found to yield a comparable level of accuracy with respect to the FE-BE approach when employing a similar number of collocation points for both methods. This, combined with the fact that SBM typically involves less Green's function evaluations with respect to BEM per collocation point, allows for concluding that the method is more computationally efficient than a standard 3D FE-BE.

- The verification study also shows that the rotational motions and bending moments must be considered in the pile-soil coupling scheme to obtain accurate results, especially when estimating the lateral response of the free field due to lateral or vertical loading patterns. The discrepancies appearing when the only translational motions and forces are considered to establish the coupling conditions are more pronounced at high frequencies.

Given the robustness of the proposed method as well as its computational efficiency merits, it conforms a interesting alternative to deal with ground vibration problems involving single piled foundations, but also to pile groups or other types of flexible foundations embedded in homogeneous or layered soils.

Appendix A. Values of the unknown constants for a pile with free-free boundary conditions

This appendix presents the expressions for the constants A_j (for $j = 1, 2, 3, 4$), B_j (for $j = 1, 2, 3, 4$), and C_j (for $j = 1, \ldots, 8$) associated to the pile model adopting free-free boundary conditions and under external unitary point loads and bending moments located at $z = z_1$, as shown in Fig. 2. The coefficients A_j are given by

$$\begin{aligned} A_1 &= -\frac{\cos(\alpha z_1)\cos(\alpha L_\mathrm{p}) + \sin(\alpha z_1)\sin(\alpha L_\mathrm{p})}{\alpha A_\mathrm{p} E_\mathrm{p} \sin(\alpha L_\mathrm{p})}, \\ A_2 &= 0, \\ A_3 &= -\frac{\cos(\alpha z_1)\cos(\alpha L_\mathrm{p})}{\alpha A_\mathrm{p} E_\mathrm{p} \sin(\alpha L_\mathrm{p})}, \\ A_4 &= -\frac{\cos(\alpha z_1)}{\alpha A_\mathrm{p} E_\mathrm{p}}. \end{aligned} \tag{A.1}$$

The coefficients B_j associated to the torsional response due to a unit torsional moment are given by

$$\begin{aligned} B_1 &= -\frac{\cos(\gamma z_1)\cos(\gamma L_\mathrm{p}) + \sin(\gamma z_1)\sin(\gamma L_\mathrm{p})}{\gamma J_\mathrm{p} G_\mathrm{p} \sin(\gamma L_\mathrm{p})}, \\ B_2 &= 0, \\ B_3 &= -\frac{\cos(\gamma z_1)\cos(\gamma L_\mathrm{p})}{\gamma J_\mathrm{p} G_\mathrm{p} \sin(\gamma L_\mathrm{p})}, \\ B_4 &= -\frac{\cos(\gamma z_1)}{\gamma J_\mathrm{p} G_\mathrm{p}}. \end{aligned} \tag{A.2}$$

Finally, the expressions for the coefficients C_j associated with the flexural response of the pile due to a unit point load are

$$\begin{aligned} C_1 &= C_3 = b_1[a_4 \sinh(\beta z_1) + a_3 \cosh(\beta z_1) + a_5 \sin(\beta z_1) + a_3 \cos(\beta z_1)], \\ C_2 &= C_4 = b_1[a_2 \sinh(\beta z_1) + a_5 \cosh(\beta z_1) + a_2 \sin(\beta z_1) + a_4 \cos(\beta z_1)], \\ C_5 &= b_1[a_4 \sinh(\beta z_1) + a_3 \cosh(\beta z_1) + a_4 \sin(\beta z_1) + a_3 \cos(\beta z_1)], \\ C_6 &= b_1[a_2 \sinh(\beta z_1) + a_5 \cosh(\beta z_1) + a_2 \sin(\beta z_1) + a_5 \cos(\beta z_1)], \\ C_7 &= b_1[a_5 \sinh(\beta z_1) + a_3 \cosh(\beta z_1) + a_5 \sin(\beta z_1) + a_3 \cos(\beta z_1)], \\ C_8 &= b_1[a_2 \sinh(\beta z_1) + a_4 \cosh(\beta z_1) + a_2 \sin(\beta z_1) + a_4 \cos(\beta z_1)]. \end{aligned} \tag{A.3}$$

where $b_1 = (a_1\beta^3)^{-1}$ and

$$\begin{aligned}
a_1 &= 4E_pI_p[\cos(\beta L_p)\cosh(\beta L_p) - 1],\\
a_2 &= \sin(\beta L_p)\cosh(\beta L_p) + \sinh(\beta L_p)\cos(\beta L_p),\\
a_3 &= \sin(\beta L_p)\cosh(\beta L_p) - \sinh(\beta L_p)\cos(\beta L_p),\\
a_4 &= \cos(\beta L_p)\cosh(\beta L_p) - \sin(\beta L_p)\sinh(\beta L_p) - 1,\\
a_5 &= -\cos(\beta L_p)\cosh(\beta L_p) - \sin(\beta L_p)\sinh(\beta L_p) + 1.
\end{aligned} \tag{A.4}$$

In the case that the flexural motion is induced by a unitary external bending moment, the coefficients C_j (for $j = 1, \ldots, 8$) become

$$\begin{aligned}
C_1 = C_3 &= b_2[a_3\sinh(\beta z_1) + a_4\cosh(\beta z_1) - a_3\sin(\beta z_1) + a_5\cos(\beta z_1)],\\
C_2 = C_4 &= b_2[a_5\sinh(\beta z_1) + a_2\cosh(\beta z_1) - a_4\sin(\beta z_1) + a_2\cos(\beta z_1)],\\
C_5 &= b_2[a_3\sinh(\beta z_1) + a_4\cosh(\beta z_1) - a_3\sin(\beta z_1) + a_4\cos(\beta z_1)],\\
C_6 &= b_2[a_5\sinh(\beta z_1) + a_2\cosh(\beta z_1) - a_5\sin(\beta z_1) + a_2\cos(\beta z_1)],\\
C_7 &= b_2[a_3\sinh(\beta z_1) + a_5\cosh(\beta z_1) - a_3\sin(\beta z_1) + a_5\cos(\beta z_1)],\\
C_8 &= b_2[a_4\sinh(\beta z_1) + a_2\cosh(\beta z_1) - a_4\sin(\beta z_1) + a_2\cos(\beta z_1)],
\end{aligned} \tag{A.5}$$

where $b_2 = (a_1\beta^2)^{-1}$.

Appendix B. Pile-soil transformation matrix

The pile-soil interaction modelling strategy is based on the assumption that the pile is divided in N_p segments, each one of them behaving as a rigid solid. Therefore, the displacement of one of these segments at the collocation points located at its perimeter can be defined in terms of the translational and rotational motions of the segment centroid. Thus, the response at the n_s-th collocation point of the n-th segment, located at the position $\mathbf{x}^{n,n_s} = \left\{ x^{n,n_s} \quad y^{n,n_s} \quad z^{n,n_s} \right\}^T$, can

be written as a function of the pile centroid point motion of the corresponding segment $\mathbf{U}_{\mathrm{p}}^{n}$ as

$$\mathbf{U}_{\mathrm{b}}^{\mathrm{p},n,n_{\mathrm{s}}} = \begin{Bmatrix} U_{\mathrm{b}x}^{n,n_{\mathrm{s}}} \\ U_{\mathrm{b}y}^{n,n_{\mathrm{s}}} \\ U_{\mathrm{b}z}^{n,n_{\mathrm{s}}} \end{Bmatrix} = \begin{bmatrix} 1 & 0 & 0 & 0 & 0 & -y^{n,n_{\mathrm{s}}} \\ 0 & 1 & 0 & 0 & 0 & x^{n,n_{\mathrm{s}}} \\ 0 & 0 & 1 & y^{n,n_{\mathrm{s}}} & -x^{n,n_{\mathrm{s}}} & 0 \end{bmatrix} \begin{Bmatrix} U_{\mathrm{p}x}^{n} \\ U_{\mathrm{p}y}^{n} \\ U_{\mathrm{p}z}^{n} \\ \theta_{\mathrm{p}x}^{n} \\ \theta_{\mathrm{p}y}^{n} \\ \theta_{\mathrm{p}z}^{n} \end{Bmatrix} = \mathbf{W}^{n,n_{\mathrm{s}}} \mathbf{U}_{\mathrm{p}}^{n}. \tag{B.1}$$

The matrix that relates the displacement at all collocation points with the six-component motions of all pile centroid points is given by

$$\mathbf{W} = \begin{bmatrix} \mathbf{W}^{1,1} & & & & & \\ \mathbf{W}^{1,2} & & & & & \\ \vdots & & & & & \\ \mathbf{W}^{1,N_{\mathrm{s}}} & & & & & \\ & \mathbf{W}^{2,1} & & & & \\ & \mathbf{W}^{2,2} & & & & \\ & \vdots & & & & \\ & \mathbf{W}^{2,N_{\mathrm{s}}} & & & & \\ & & \ddots & & & \\ & & & \mathbf{W}^{N,1} & & \\ & & & \mathbf{W}^{N,2} & & \\ & & & \vdots & & \\ & & & \mathbf{W}^{N,N_{\mathrm{s}}} & & \\ & & & \mathbf{W}^{N,N_{\mathrm{s}}+1} & & \end{bmatrix}. \tag{B.2}$$

It can be demonstrated that the transpose of this matrix can be also used to determine the equivalent forces applied at the segment centroid as a result of the forces at the collocation points, giving

$$\mathbf{P}_{\mathrm{p}} = -\mathbf{W}^{\mathrm{T}} \mathbf{P}_{\mathrm{b}}^{\mathrm{s}}. \tag{B.3}$$

In the case that neither the rotations nor the bending and torsion moments associated with each segment are included in the coupling procedure, the right-hand 3×3 matrix of $\mathbf{W}^{n,n_{\mathrm{s}}}$ should be replaced by a null matrix.

Appendix C. Vertical and lateral soil reaction equations

In the approximate formulation presented by Baranov [4], the soil reactions are described by

$$\begin{aligned} N_x &= GS_x u(z), \\ N_z &= GS_z w(z), \end{aligned} \tag{C.1}$$

where N_x and N_z are, respectively, the soil reactions to lateral and vertical motions, G is the shear modulus of the soil and S_x and S_z are given by

$$\begin{aligned} S_x(a_0, \nu) &= 2\pi a_0 \frac{\frac{1}{\sqrt{q}} H_2^{(2)}(a_0) H_1^{(2)}(x_0) + H_2^{(2)}(x_0) H_1^{(2)}(a_0)}{H_0^{(2)}(a_0) H_2^{(2)}(x_0) + H_0^{(2)}(x_0) H_2^{(2)}(a_0)}, \\ S_z(a_0) &= 2\pi a_0 \frac{J_1(a_0) J_0(a_0) + Y_1(a_0) Y_0(a_0)}{J_0^2(a_0) + Y_0^2(a_0)} + \frac{4\mathrm{i}}{J_0^2(a_0) + Y_0^2(a_0)}, \end{aligned} \tag{C.2}$$

where $H_n^{(2)}$ is the Hankel function of the second kind and order n, J_0 and J_1 are the Bessel functions of the first kind of order zero and one, respectively, and Y_0 and Y_1 are the Bessel functions of the second kind of order zero and one, respectively. The dimensionless frequency a_0 and the parameters q and x_0 are given by

$$a_0 = r_\mathrm{p} \omega \sqrt{\frac{\rho}{G}}, \quad q = \frac{(1 - 2\nu)}{2(1 - \nu)}, \quad x_0 = a_0 \sqrt{q}, \tag{C.3}$$

where r_p is the pile radius, ω the angular frequency, ρ is the density of the soil and ν its Poisson's ratio.

Acknowledgements

This research has been carried out with the financial support of three research projects:

- Project VIBWAY: Fast computational tool for railway-induced vibrations and re-radiated noise assessment, with reference RTI2018-096819-B-I00, supported by the MCIN/AEI/10.13039/501100011033 and FEDER "*Una manera de hacer Europa*".
- Programmatic funding UIDP/04708/2020 of the CONSTRUCT (Instituto de I&D em Estruturas e Construções), funded by national funds through the FCT/MCTES (PIDDAC).
- Project PTDC/ECI-CON/29634/2017 (POCI-01-0145-FEDER-029634) and project PTDC/ECI-EGC/3352/2021, both funded by FEDER funds through COMPETE2020, Programa Operacional Competitividade e Internacionalização

(POCI), and by national funds (PIDDAC) through FCT/MCTES.

The first author would like to thank the "Programa Nacional de Becas y Crédito Educativo" PRONABEC (www.pronabec.gob.pe) for the financial support given through the scholarship "Generación del Bicentenario de la República del Perú". Furthermore, the authors would like to gratefully acknowledge the support of Mrs. Mònica Sabrià Miracle to locate a copy of the paper [4].

References

[1] K. A. Kuo, H. Hunt, Dynamic models of piled foundations, Appl. Mech. Rev. 65 (2013) 9, doi:10.1115/1.4024675.

[2] M. Novak, Dynamic stiffness and damping of piles, Can. Geotech. J. 11 (1974) 574–598, doi:10.1139/t74-059.

[3] J. Lysmer, F. E. Richart, Dynamic response of footings to vertical loading, J. Soil Mech. Found. Div 92 (1966) 65–91, doi:10.1061/JSFEAQ.0000846.

[4] V. A. Baranov, On the calculation of excited vibrations of an embedded foundation (in Russian), Vopr. Dynamiki Prochnocti 14 (1967) 195–209.

[5] M. Novak, Y. O. Beredugo, Vertical vibration of embedded footings, J. Soil Mech. Found. Div. Proc. Am. Soc. Civ. Eng. 98 (1972) 1291–1310, doi:10.1061/JSFEAQ.0001815.

[6] Y. O. Beredugo, M. Novak, Coupled horizontal and rocking vibration of embedded footings, Can. Geotech. J. 9 (1972) 477–497, doi:10.1139/t72-046.

[7] M. Novak, R. Grigg, Dynamic Experiments With Small Pile Foundations, Can. Geotech. J. 13(4) (1976) 372–385, doi:10.1139/t76-039.

[8] A. M. Kaynia, E. Kausel, Dynamics of piles and pile groups in layered soil media, Soil Dyn. Earthq. Eng. 10 (1991) 386–401, doi:10.1016/0267-7261(91)90053-3.

[9] E. Ntotsios, W. Hamad, D. Thompson, M. Hussein, H. Hunt, J. Talbot, Predictions of the dynamic response of piled foundations in a multi-layered half-space due to inertial and railway induced loadings, in: 5th International Conference on Computational Methods in Structural Dynamics and Earthquake Engineering (COMPDYN), 24–26 May 2015, Rhodes, Greece, pp. 133–145.

[10] T. Nogami, M. Novak, Soil-pile interaction in vertical vibration, Earthq. Eng. Struct. Dyn. 4 (1976) 277–293, doi:10.1002/eqe.4290040308.

[11] T. Nogami, M. Novak, Resistance of soil to a horizontally vibrating pile, Earthq. Eng. Struct. Dyn. 5 (1977) 249–261, doi:10.1002/eqe.4290050304.

[12] M. Novak, Vertical Vibration of floating piles, J. Eng. Mech. Div. 103 (1977) 153–168, doi:10.1061/JMCEA3.0002201.

[13] R. Y. S. Pak, P. C. Jennings, Elastodynamic response of pile under transverse excitations, J. Eng. Mech. 113(7) (1987) 1101–1116, doi:10.1061/(ASCE)0733-9399(1987)113:7(1101).

[14] J. P. Wolf, Foundation vibration analysis using simple physical models, Prentice-Hall, London, United Kingdom (1995).

[15] R. K. N. D. Rajapakse, A. H. Shah, On the longitudinal harmonic motion of an elastic bar embedded in an elastic half-space, Int. J. Solids Struct. 23(2) (1987) 267–285, doi:10.1016/0020-7683(87)90060-6.

[16] R. K. N. D. Rajapakse, A. H. Shah, On the lateral harmonic motion of an elastic bar embedded in an elastic half-space, Int. J. Solids Struct. 23(2) (1987) 287–303, doi:10.1016/0020-7683(87)90061-8.

[17] G. Anoyatis, R. Di Laora, A. Mandolini, G. Mylonakis, Kinematic response of single piles for different boundary conditions: Analytical solutions and normalization schemes, Soil Dynamics and Earthquake Engineering 44 (2013) 183–195, doi:https://doi.org/10.1016/j.soildyn.2012.09.011.

[18] G. Anoyatis, R. Di Laora, G. Mylonakis, Axial kinematic response of end-bearing piles to p waves, International Journal for Numerical and Analytical Methods in Geomechanics 37 (2013) 2877–2896, doi:https://doi.org/10.1002/nag.2166.

[19] R. D. Laora, E. Rovithis, Kinematic bending of fixed-head piles in nonhomogeneous soil, Journal of Geotechnical and Geoenvironmental Engineering 141 (2015) 04014126, doi:10.1061/(ASCE)GT.1943-5606.0001270.

[20] R. D. Laora, E. Rovithis, Kinematic bending of fixed-head piles in nonhomogeneous soil, Journal of Geotechnical and Geoenvironmental Engineering 141 (2015) 04014126, doi:10.1061/(ASCE)GT.1943-5606.0001270.

[21] K. A. Kuo, H. E. M. Hunt, An efficient model for the dynamic behaviour of a single pile in viscoelastic soil, J. Sound Vib. 332 (2013) 2549–2561, doi:10.1016/j.jsv.2012.12.023.

[22] J. A. Forrest, H. E. M. Hunt, A three-dimensional tunnel model for calculation of train-induced ground vibration, J. Sound Vib. 294 (2006) 678–705, doi:10.1016/j.jsv.2005.12.032.

[23] J. A. Forrest, H. E. M. Hunt, Ground vibration generated by trains in underground tunnels, J. Sound Vib. 294 (2006) 706–736, doi:10.1016/j.jsv.2005.12.031.

[24] R. Krishnan, G. Gazetas, A. Velez, Static and dynamic lateral deflexion of piles in non-homogeneous soil stratum, Geotechnique 33 (1983) 307–325, doi:10.1680/geot.1983.33.3.307.

[25] A. Velez, G. Gazetas, R. Krishnan, Lateral dynamic response of constrained-head piles, J. Geotech. Eng. 109 (1983) 1063–1081, doi:10.1061/(ASCE)0733-9410(1983)109:8(1063).

[26] G. Wu, W. D. Finn, Dynamic nonlinear analysis of pile foundations using finite element method in the time domain, Can. Geotech. J. 34 (1997) 44–52, doi:10.1139/t96-088.

[27] B. K. Maheshwari, K. Z. Truman, M. H. El Naggar, P. L. Gould, Three-dimensional finite element nonlinear dynamic analysis of pile groups for lateral transient and seismic excitations, Can. Geotech. J. 41 (2004) 118–133, doi:10.1139/t03-073.

[28] B. K. Maheshwari, K. Z. Truman, P. L. Gould, M. H. El Naggar, Three-Dimensional Nonlinear Seismic Analysis of Single Piles Using Finite Element Model: Effects of Plasticity of Soil, Int. J. Geomech. 5 (2005) 35–44, doi:10.1061/(asce)1532-3641(2005)5:1(35).

[29] K. J. Bentley, M. H. E. Naggar, Numerical analysis of kinematic response of single piles, Can. Geotech. J. 37 (2000) 1368–1382, doi:10.1139/cgj-37-6-1368.

[30] R. Kuhlemeyer, Static and dynamic laterally loaded floating piles, J. Geotech. Eng. Div. Proc. Am. Soc. Civ. Eng. 105 (1979) 289–304, doi:10.1061/AJGEB6.0000771.

[31] R. Kuhlemeyer, Vertical vibration of piles, J. Geotech. Eng. Div. Proc. Am. Soc. Civ. Eng. 105 (1979) 273–287.

[32] K. Syngros, Seismic response of piles and pile-supported bridge piers evaluated through case histories, Ph.D. thesis, The City University of New York, 2004.

[33] A. F. Homayoun Rooz, A. Hamidi, A numerical model for continuous impact pile driving using ale adaptive mesh method, Soil Dynamics and Earthquake Engineering 118 (2019) 134–143, doi:https://doi.org/10.1016/j.soildyn.2018.12.014.

[34] A. Colaço, P. A. Costa, C. M. Parente, A. S. Cardoso, Ground-borne noise and vibrations in buildings induced by pile driving: An integrated approach, Applied Acoustics 179 (2021) 108059, doi:10.1016/j.apacoust.2021.108059.

[35] J. Lysmer, R. L. Kuhlemeyer, Finite dynamic model for infinite media, J. Mech. Div. 95 (1969) 859–877, doi:10.1061/JMCEA3.0001144.

[36] D. E. Beskos, Boundary element methods in dynamic analysis, Appl. Mech. Rev. 40 (1987) 1–23, doi:10.1115/1.3149529.

[37] D. E. Beskos, Boundary element methods in dynamic analysis: Part II (1986-1996), Appl. Mech. Rev. 40 (1987) 1–23, doi:10.1115/1.3149529.

[38] S. E. Kattis, D. Polyzos, D. E. Beskos, Vibration isolation by a row of piles using a 3-D frequency domain BEM, Int. J. Numer. Methods Eng. 46 (1999) 713–728, doi:10.1002/(SICI)1097-0207(19991020)46:5¡713::AID-NME693¿3.0.CO;2-U.

[39] L. A. Padrón, J. J. Aznárez, O. Maeso, BEM-FEM coupling model for the dynamic analysis of piles and pile groups, Eng. Anal. Bound. Elem. 31 (2007) 473–484, doi:10.1016/j.enganabound.2006.11.001.

[40] J. P. Talbot, H. E. M. Hunt, A computationally efficient piled-foundation model for studying the effects of ground-borne vibration on buildings, Proc. Inst. Mech. Eng. Part C J. Mech. Eng. Sci. 217 (2003) 975–990, doi:10.1243/095440603322407227.

[41] P. Coulier, The vibration response of piled foundations to inertial and underground railway induced loadings, 2010.

[42] T. L. Edirisinghe, J. P. Talbot, Inertial interaction in pile-groups: A study of the influence of coupling via an iterative wave-scattering approach, Comput. Geotech. 128 (2020) 103804, doi:10.1016/j.compgeo.2020.103804.

[43] W. Chen, F. Z. Wang, A method of fundamental solutions without fictitious boundary, Eng. Anal. Bound. Elem. 34 (2010) 530–532, doi:10.1016/j.enganabound.2009.12.002.

[44] Y. Gu, W. Chen, C.-Z. Zhang, Singular boundary method for solving plane strain elastostatic problems, International Journal of Solids and Structures 48 (2011) 2549–2556, doi:10.1016/j.ijsolstr.2011.05.007.

[45] Y. Gu, W. Chen, Z. J. Fu, B. Zhang, The singular boundary method: Mathematical background and application in orthotropic elastic problems, Eng. Anal. Bound. Elem. 44 (2014) 152–160, doi:10.1016/j.enganabound.2014.02.001.

[46] L. Sun, W. Chen, A. H. Cheng, Singular boundary method for 2D dynamic poroelastic problems, Wave Motion 61 (2016) 40–62, doi:10.1016/j.wavemoti.2015.10.004.

[47] H. Liravi, R. Arcos, A. Clot, K. F. Conto, J. Romeu, A 2.5D coupled FEM–SBM methodology for soil–structure dynamic interaction problems, Engineering Structures 250 (2022) 113371, doi:10.1016/j.engstruct.2021.113371.

[48] M. Bonnet, Boundary integral equation methods for solids and fluids, John Wiley and Sons, Chichester, United Kingdom (1995).

[49] J. Lin, W. Chen, C. S. Chen, Numerical treatment of acoustic problems with boundary singularities by the singular boundary method, J. Sound Vib. 333 (2014) 3177–3188, doi:10.1016/j.jsv.2014.02.032.

[50] E. Kausel, Fundamental solutions in elastodynamics: A compendium, Cambridge University Press, 2006.

[51] W. Chen, Y. Gu, An improved formulation of singular boundary method, Advances in Applied Mathematics and Mechanics 4 (2012) 543–558, doi:10.4208/aamm.11-m11118.

[52] Z. Fu, W. Chen, J. Chen, W. Qu, Singular boundary method: Three regularization approaches and exteriorwave applications, CMES - Computer Modeling in Engineering and Sciences 100 (2014) 59–84, doi:10.3970/cmes.2014.099.255.

[53] A. M. Kaynia, Dynamic stiffness and seismic response of pile groups, Ph.D. thesis, Massachusetts Institute of technology, 1982.

[54] International Organization for Standardization, ISO 14837-1. Mechanical vibration. Ground-borne noise and vibration arising from rail systems. Part 1: General Guidance, 2005.

[55] M. Schevenels, S. François, G. Degrande, EDT: An ElastoDynamics Toolbox for MATLAB, Comput. Geosci. 35 (2009) 1752–1754, doi:10.1016/j.cageo.2008.10.012.

[56] J. Domínguez, R. Abascal, On fundamental solutions for the boundary integral equations method in static and dynamic elasticity, Eng. Anal. 1 (1984) 128–134.

[57] U. Basu, A. K. Chopra, Perfectly matched layers for time-harmonic elastodynamics of unbounded domains: theory and finite-element implementation, Computer Methods in Applied Mechanics and Engineering 192 (2003) 1337–1375, doi:https://doi.org/10.1016/S0045-7825(02)00642-4.

[58] S. François, M. Schevenels, G. Lombaert, G. Degrande, A 2.5 D displacement-based PML for elastodynamic wave propagation, in: Proceedings of the 4th European Conference on Computational Mechanics.

[59] Z.-J. Fu, W. Chen, J. Lin, A. H.-D. Cheng, Singular boundary method for various exterior wave applications, International Journal of Computational Methods 12 (2015) 1550011, doi:10.1142/S0219876215500115.